On limited Predictability

By A. WIIN-NIELSEN

Matematisk-fysiske Meddelelser **47**

Det Kongelige Danske Videnskabernes Selskab
The Royal Danish Academy of Sciences and Letters

Abstract

The limited predictability experienced by extended integrations of the nonlinear equations governing a large class of systems is illustrated by a number of examples. Lacking a general theory permitting an estimate of the limits of the predictability for a given system the strategy is to compare two numerical integrations starting either from slightly different initial states or from identical initial states, but with small changes in the forcing.

The difference between the practical and the theoretical limits of predicitability is discussed. The theoretical limit may be determined by starting from two initial states with only infinitesimal differences or from similar differences in the forcing, while the practical limit is determined by the uncertainty of the initial state due to the accuracy and distributions of observations and by the uncertainty in describing the forcing of a given system.

By A. Wiin-Nielsen
Niels Bohr Institute for Astronomy, Physics and Geophysics
Department of Geophysics
Juliane Maries Vej 30
2100 Copenhagen, Denmark.

Printed in Denmark by Special-Trykkeriet Viborg a-s
ISSN 0023-3323. ISBN 87-7304-185-8

1. Introduction

The equations of classical physics are deterministic providing one and only one solution for a given initial state and a given forcing. The independent variables are normally three space coordinates and one time coordinate. The dependent variables are in general the three components of the velocity, the pressure, the density and the temperature, but in many cases a reduced set of independent and dependent variables have been used. The solution of the classical two-body astronomical problem requires only the basic Newtonian law that mass times acceleration is equal to the sum of forces acting on the mass. Geophysical modeling has also developed over several decades, going from the simple to the more complicated. In some cases it is necessary to supplement the basic six dependent variables by additional variables because the system under consideration may require special treatment of one of its components. As an example it may be mentioned that a realistic treatment of the atmosphere of the Earth requires a special equation for the content of water vapour. Otherwise it is not possible to treat the cloud and precipitation processes.

From the times of Newton to about 1890 it was generally believed that if one knows the initial state with great accuracy, and if all the forces acting on a given system can be formulated with equal accuracy, it would be possiple, in principle, to make predictions of the state of the universe for an infinitely long time.

The limited predictability of physical systems has been known for about a century. The first discussion of the concept, known by the author, was given by Poincaré (1893 and 1912). He discussed in particular the limited predictability in the three body astronomical problem indicating that small changes in the initial state could result in large changes in the trajectories of the three bodies during the numerical integration of the three relevant equations. A single example of such an integration is presented in the appendix to this paper.

The best known example of both theoretical and operational limited predictability is the weather prediction problem simply because objective numerical weather predictions using various models based on the atmospheric dynamics have been in operation for almost half a century. Thompson (1957) was the first to analyse the limited predictability due to the uncertainties in the initial field. Since these predic-

tions have been verified for a long time it has been possible to follow the gradual increase of the operational predictability from a single to several days. Within the field of weather predictions we have also some estimates of the theoretical limit of predictability. The weather prediction problem will be discussed in Section 2 of this paper.

In other geophysical areas we have much less information about predictability. The reason is of course that no other area has experienced the same systematic development and use of observational systems for predictions as has been the case in the atmospheric sciences. On the other hand, atmospheric prediction models have been developed to a state where information about the upper layers of the oceans, the distribution of land and sea ice, the topography and the vegetation of the continents are necessary for a proper determination of the initial state for an atmospheric prediction and for the interactive processes during the numerical integration of the model equations. Chaos is equivalent to limited predictability simply because chaos is defined as sensitivity to small changes in the initial state.

The predictions mentioned so far are attempts to forecast a future state in as much detail as possible. The numerical integrations may be based on a grid-point model, a spectral model or a combination of the two in the sense that a spectral model is used for the time integrations, while a grid-point model is used to determine the influence of local processes on the forcing of the model. The reason for such an arrangement is that the spectral equations may be integrated with great accuracy, but to incorporate processes on a small scale at a given locality it is necessary to know local changes with great accuracy. In the latter case it is necessary to have effective and accurate programs to go back and forth between the two kinds of representation. Such programs, depending on fast Fourier transforms, have been developed.

A second kind of desirable prediction is to predict a future averaged state of a system. The goals could for example be to make monthly predictions, seasonal predictions or simulations of various climatic states. A direct approach to this problem is to integrate a suitable model for a sufficiently long time whereafter the appropriate time average is computed as the end product. In view of the limited predictability one may ask if this procedure will lead to a suitable and useful prediction. It is of course realized that the transient, relatively short waves after such a long integration will not be found in the correct place and with a suitable amplitude. However, the time average will to a large extent eliminate the transient waves and the final product should thus in addition to the zonal state contain mainly the very long waves which are forced by the topography and the heat sources. If this argument is correct, it may be asked if one could not just as well use a spectral model containing only components describing the smaller wave numbers, i.e. the large planetary scales. This possibility requires that the shorter transient waves do not

feed energy into the longer waves, but diagnostic studies of the energy transfers in the spectral domain conducted by Lin and Derome (1995) indicates that the largest scale waves do indeed receive energy from the shorter transient waves indicating that a lower order model, treating only the large planetary scales, is not a viable possibility. A second possibility is to avoid the major nonlinear terms by averaging the equations over the whole globe. The major nonlinear terms average to zero in this case, and the remaining equations are much easier to handle. The disadvantage of this procedure is that one will also have to deal with the physical processes in an average way. It is thus not possible to pay attention to size and position of the continents and the oceans. However, this approach may be used as a supplement to the very long integrations of the original equations for the model. Thus, the problems of predictions of the second kind has not so far been solved in a satisfactory way.

The determination of the practical limit for atmospheric predictability requires a large number of cases of global integrations. Reliable results can be obtained only from institutions engaged in the production of such forecasts. To illustrate limited predictability it is possible to select various low order models and use the integrations of the model equations to demonstrate the main nature of the phenomenon. Since these model contain only a few components, they will not be able to pay attention to the nonlinear cascades of energy in the spectrum. Some low-order models will be defined and used in Section 3 of this paper.

2. Atmospheric predictions

Atmospheric predictions were for a long time based on the experience of the forecaster and on empirical and statistical rules. Such forecasts were normally limited to 1 or 2 days. With the availability of the first computers appearing in the late 1940's it became possible for the first time to attempt atmospheric forecasts based on simple models of the dynamics of the atmosphere. The very first model, formulated in 1949, used the vorticity equation applied to the vertically averaged atmosphere. This simple barotropic model assuming quasi-geostrophic or quasi-nondivergent flow was later replaced by models using several levels to describe the vertical structure of the atmosphere. The first models had neither energy sources nor dissipation. They could generally be used for a couple of days and were often integrated on grids covering less than a hemisphere.

These models were later replaced by more complete hemispheric and global models using the primitive equations. A description of the general development has been given by the author (Wiin-Nielsen, 1997). Present models for short- and medium-range prediction are typically global with a large number of levels to describe the vertical variations of the atmosphere. The best models has a horizontal

resolution permitting wavelengths as small as 200 km. The models contain heat sources and sinks as well as friction in the boundary layer and the free atmosphere. The radiation budgets for the incoming short wave radiation and the outgoing long wave radiation are a part of the model. The orography is included with a resolution corresponding to the horizontal resolution of the model. Special quantities are necessary at the surface such as ground and sea roughness, ground and sea surface temperatures, ground humidity, snow-cover and sea ice. Gravity wave drag, evaporation, transfer of sensible and latent heat flux are included. The clouds are divided in high, medium, low and convective clouds. One deals with both stratiform and convective precipitation as well as an almost complete water budget at the surface and sub-surface levels.

The status of numerical weather prediction about 15 years ago is given by Bengtsson (1985). Figure 1a compares short-range predictions made by various institutions. The measure of accuracy is here the RMS-difference between the forecast and the observed state. The differences are to a large extent explained by the computer capacity available to the national meteorological centers. A small capacity means larger gridsizes and perhaps less than hemipheric forecast regions with ar-

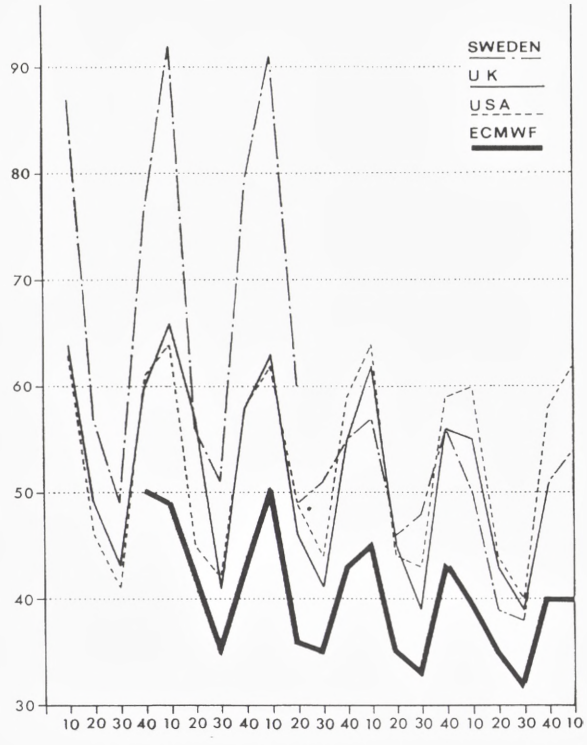

Fig. 1a: The RMS-errors for predictions from various organizations for the years 1979 to 1983.

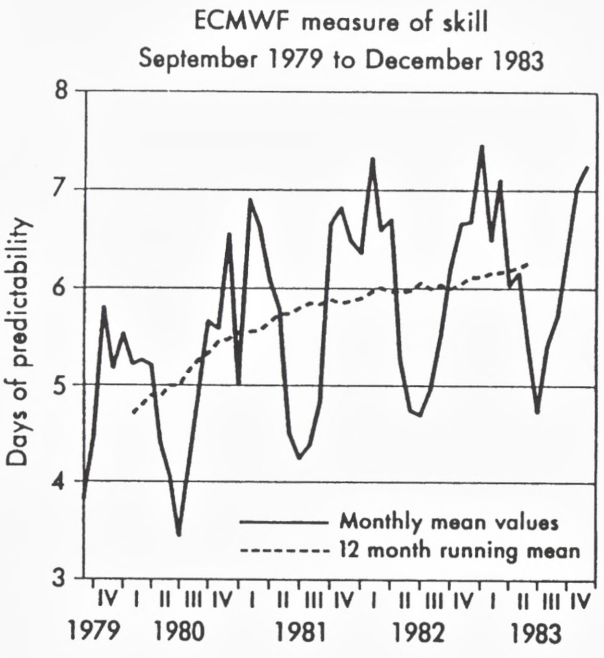

Fig. 1b: The number of days of predictability, defined as those for which the 500 hPa height anomaly correlation coefficient exceeds 0.6. The anomaly is defined as the deviation from the mean for the period.

tificial boundary conditions. Figure 1b shows the development of atmospheric predictability from late 1979 to 1983. The predictability is determined by the time at which the anomaly correlation goes below the value 0.6. The value of 0.6 is selected because practical experience shows that this value represents an accuracy where the forecast is still useful for meteorological operations. A value of 0.8 is occasionally used. The operational predictability times becomes shorter in this case. The 12 months running mean (dashed curve) shows an increase in practical predictability from about 4 days to 6 days. The solid curve, based on monthly mean values, indicate that the limit of predictability varies during the year with the largest predictability in winter and the smallest in summer. This is most likely due to the fact that the important weather processes are on a smaller scale during the summer than during the winter. The model on which the curves are based had a rather coarse resolution which did not permit the proper representation of the smaller scale dynamical processes during the summer. Later models with higher spatial resolution has decreased or eliminated this annual variation in accuracy.

The dependence of operational predictability on scale for the same early model is demonstrated in Figure 2, where the predictability is determined for short (wave numbers 10 to 20), medium (wave numbers 4 to 9) and long (wave numbers 1 to 3) waves. The results apply to a single winter month (January, 1983). The increase of practical predictability for the years 1972-1992 is shown in Figure 3. Measured

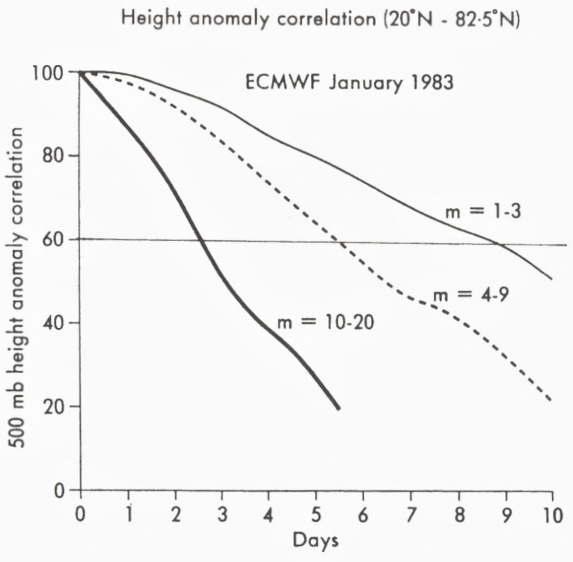

Fig. 2: The 500 hPa anomaly correlation for the region 20 to 82.5 deg. north for very long waves (wave numbers 1-3), medium waves (wave numbers 4-9) and short waves (wave numbers 10-20) for January 1983. The predictability varies from less than three days for the short waves to about 9 days for the longest waves.

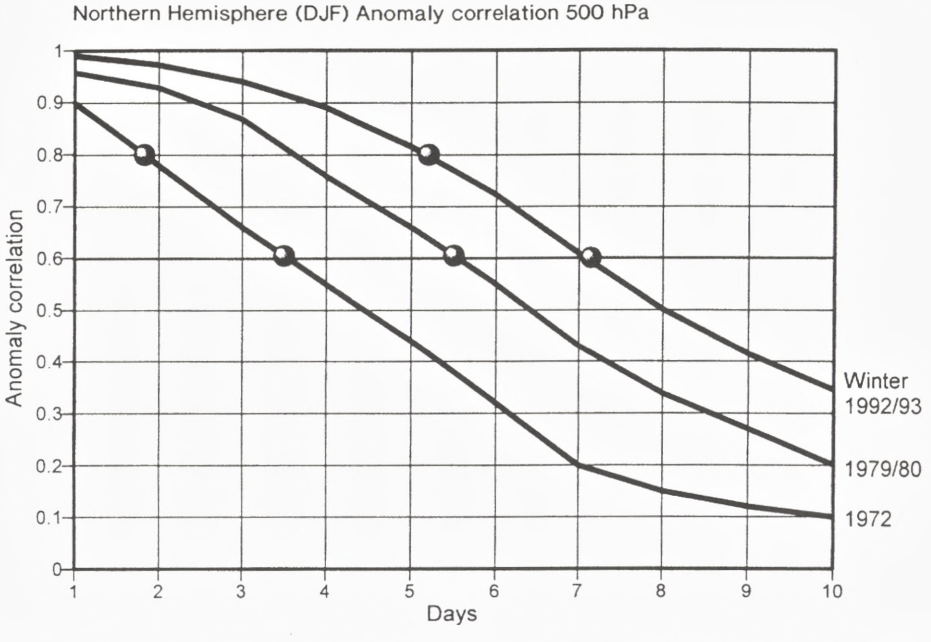

Fig. 3: The anomaly correlation for the Miyakoda forecasts 1972, the ECMWF forecasts for 1979/80 and for 1992/93, showing a predictability of 7 days.

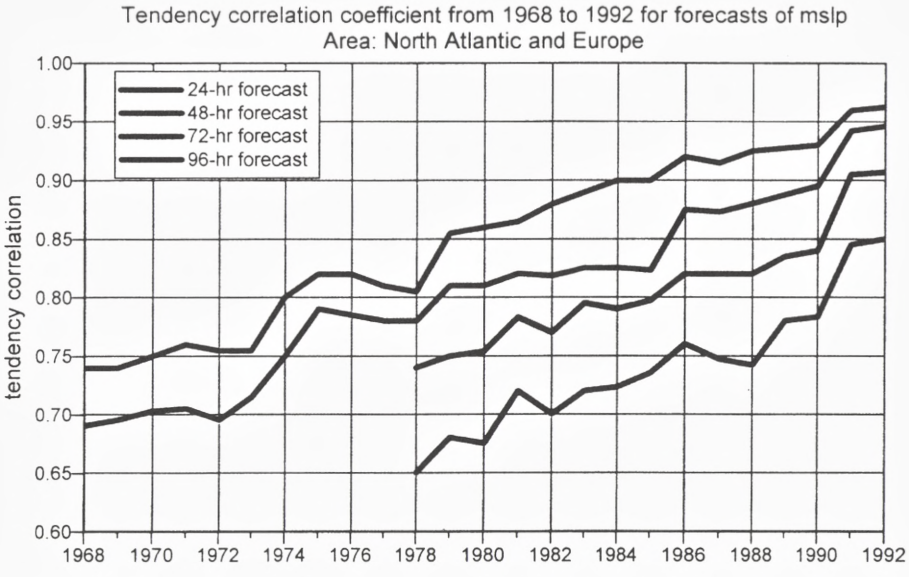

Fig. 4a: A comparison of the accuracy of forecasts for 1 day (upper curve) to 4 days (lower curve) for the interval from 1968 to 1992. Note for example that the 4 day forecast in 1992 is as good as the 1 day forecast in 1979.

again by the lower limit of 0.6 for the anomaly coefficient we find an increase from about 3.5 days to about 7 days. Figure 4a shows the changes in accuracy for one, two, three and four day forecasts. The uppermost curve applies to 24 hour forecasts and lowest curve to 96 hour forecasts. It may for example be noted that by 1992 the four day forecast was as good as the one day forecast in 1979. Figure 4b is similar to Figure 3, but is based on later information bringing the error curve to the winter 1997/98. Further progress is noted by comparing Figure 3 and Figure 4b. The practical limit for acceptable forecasts is now almost 8 days. Since a part of the contribution to forecast errors come from the uncertainty in the initial state, it may be an advantage to make a number of forecasts from slightly different initial states. Each of these forecasts will be different for a given verification time. The average of all the forecasts may be a better forecast than any of the single forecasts. Figure 4c is similar to Figure 4b, but the ensemble mean forecast has been tested against the analyses for the later part of the 10 day forecasts. It is seen that using the ensemble procedure the limit for acceptable forecasts is extended to almost 9 days. It is stressed that all the figures refer to averages. They are therefore not valid for individual forecasts which may be better or worse.

After this discussion of the practical limits of predictability it should be mentioned that the theoretical limit of predictability for the atmosphere may be esti-

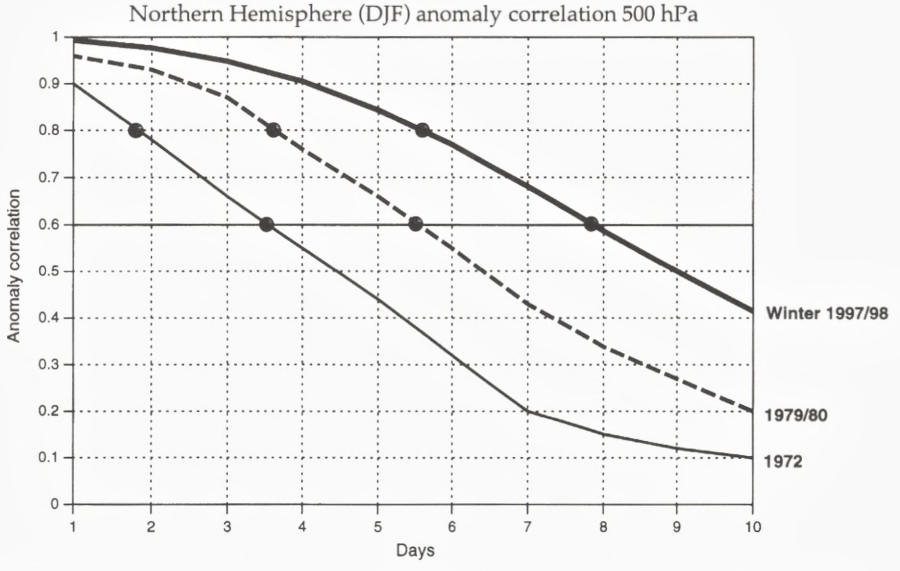

Fig. 4b: The increase of the predictability from 1972 (3.5 days) to 1997/98 of almost 8 days.

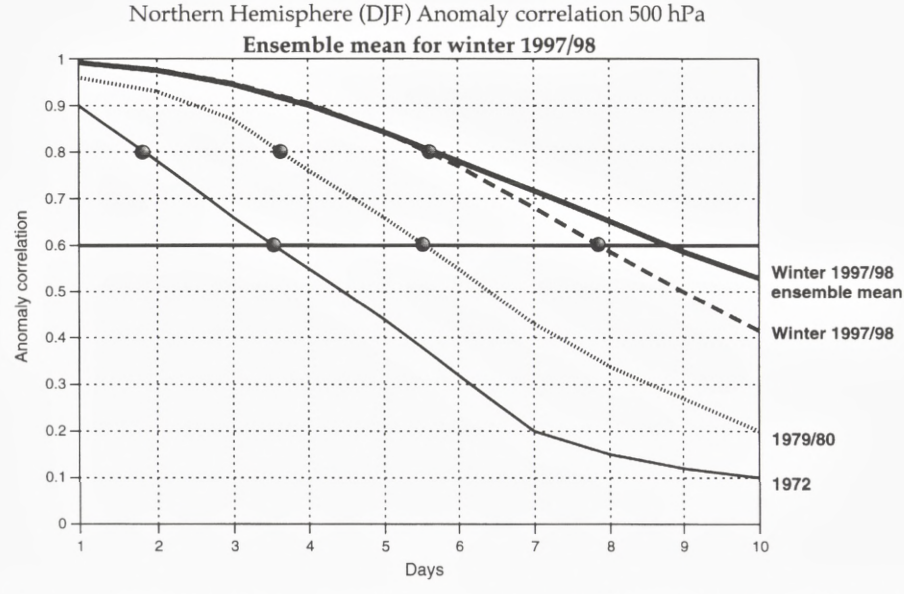

Fig. 4c: As Figure 4b, but the ensemble forecast for the winter 1997/98 has been added to the figure showing a predictability of almost 9 days.

mated by making two long integrations starting from initial states which are almost identical. The initial states differ only by infinitesimal amounts. The problem is thus to determine when the difference between the two integrations become too large. The first attempts were made as early as 1966 as part of the preparation for the Global Weather Experiment (Charney, 1966). Such experiments are not easy to carry out. The initial difference was introduced in the temperature fields as a single wave component in the baroclinically unstable region. Three different models were used. If the difference between the two initial states is very small, the dissipation in the model will have a tendency to eliminate the difference. One of the models gave indeed the result that the difference between the two forecasts increased in the early part of the integration, but decreased then to small values. Nevertheless, a certain estimate was made based on one of the models, and the result was a theoretical limit of predictability of 15 to 19 days. Since then models have become better both with respect to the parameterization of the physical processes and the vertical and horizontal resolution. It may be worthwhile to attempt a new determination of the theoretical limit of predictability using the best global models.

Some information about the theoretical limit of predictability may also be obtained from Figure 4d. The various curves give the root-mean-square errors (RMSE) for various experiments. The top dashed curve shows the RMSE values

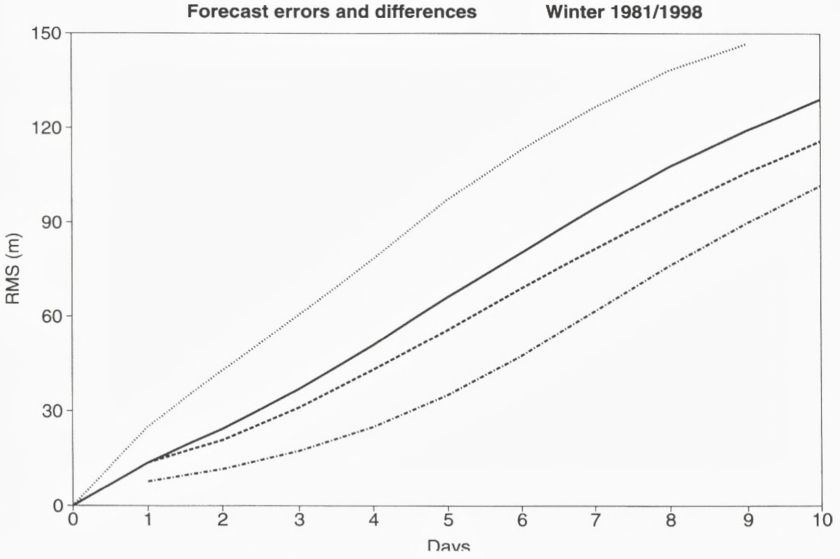

Fig. 4d: The top curve is the RMS-error as a function of time for forecasts prepared in 1981 (dotted curve), while the solid curve is the Rms-errors for 1998. The dashed curve indicates the Rms-errors which would be obtained if the model errors could be removed, while the lowest curve estimates the RMS-errors if the errors in the initial state could be greatly reduced.

for the winter 1980/81 as a function of time measured in days. The solid curve is the RMSE values for the winter 1997/98 indicating the improvements of the forecasts over 17 years of operational predictions. The third (dashed) curve from the top is obtained by removing the model errors beyond Day 1. It shows in other words the potential skill, if the model was perfect, while the forecasts still are influenced by the uncertainty in the initial state. The lowest (dashed-dotted) curve indicates the potential skill if the erorrs at day 1 was further reduced by as much as the reduction experienced from 1980/81 to 1997/98. If such an improvement could be obtained a further extention of the operational predictability would be possible. In this imagined situation even the 10 day forecasts would be useful.

The curves in Figure 4d are limited to 10 days because the daily operational forecasts are not carried beyond this time. A theoretical limit of predictability could be obtained if the forecasts on an experimental basis were carried so far into the future that the three lowest curves converged. Such experiments may be carried out in the future.

The reason for the present operational limit of predictability is that the observations do not permit an initial analysis without errors. In addition, the description of the many physical processes in the atmosphere necessary to determine the net heating is done by parameterizing small scale processes in terms of the gridpoint variables used in the model. Such a process cannot be without errors since it depends on empirical and statistical procedures. It is most likely that the latest gain in operational predictability is due to better atmospheric observations, particularly the information from satellites, because the improvements are seen also for the forecasts for the shorter periods.

3. Limited predictability in simple geophysical models

Since no general theory is known for limited predictability it will be necessary to illustrate the behavior by selecting various examples. They will be based on low-order models where the integrations can be carried out with ease. Low-order models have limitations. They contain the nonlinear interactions among the spectral components in a rudimentary form only. Therefore, they do not have cascade processes linking the spectral region of the large-scale forcing with the dissipation range. Nevertheless, they are convenient tools that can illustrate the occasionally unexpected behavior due to the nonlinear nature of the models.

Example A: Lorenz attractor

We select the well known strange Lorenz attractor as the first example. It has been described in many references such as Lorenz (1963, 1989). The equations for the

model are given in (3.1) using the standard notations. We recall that the model decribes convection between two horizontal plates.

$$\frac{dx}{dt} = \sigma\,(y-x)$$

$$\frac{dy}{dt} = xz+rx-y \qquad (3.1)$$

$$\frac{dz}{dt} = xy-bz$$

The standard case will be used. It has b=8/3 and σ=10. r is the Rayleigh number, and it is proportional to the temperature difference between the lower and the upper horizontal plates. The theory for the convection says that if r<1 we get molecular transfer of heat from the lower to the upper plate. For r>1, but not too large, convection cells develop between the plates. When 1<r<r_c (r_c = 24.74) the equations have one unstable state (0,0,0) and two steady states, while r>r_c results in three unstable steady states. In the latter case the system will never come to rest. On the other hand, it can be shown that the system cannot go to infinity because being sufficiently far away from (0,0,0) it will move back towards this point.

We select first r=28. It is in the region containing three unstable steady state. An integration from a given initial state is carried out. A second integration with r_1 = 28.001 from the same initial state is included in the program. Let the variables in the second integration be denoted (u,v,w). As a measure of the difference between the two integration we may use the rms-value given in (3.2).

$$d=[(x-u)^2+(y-v)^2+(z-w)^2]^{1/2} \qquad (3.2)$$

With a starting position for both integrations in (0,0.01,0) integrations were carried out for 40 time units. The difference as measured by (3.2) is shown in Figure 5. Between 20 and 25 time units we notice that the two solutions are definitely different. The difference between them changes in time, but the two solutions do not come close to each other again.

When we select a value of r<r_c we know that two steady states will be present. A detailed discussion of this case has been given by Wiin-Nielsen, (1998). Naturally, if we select the initial state very close to one of the steady states an integration will end in the steady state. On the other hand, for an initial state far from the two steady states we cannot in advance say, if the integration will lead to any of the steady states, and, if it does, which steady state will be approached. Figure 6a shows the

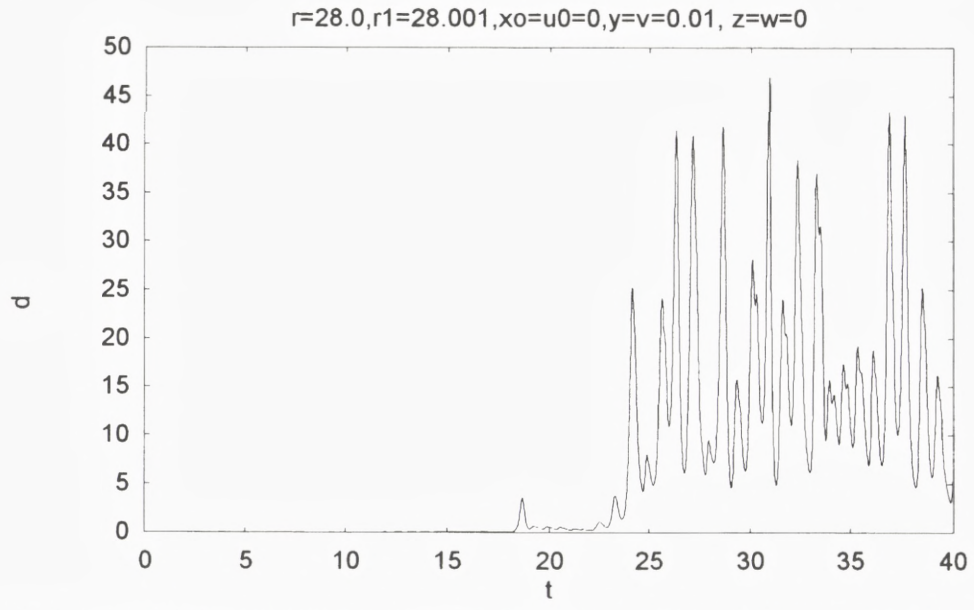

Fig. 5: The RMS-difference between two integrations of the Lorenz-model if the forcing is changed by 0.001. The predictability is lost between 20 and 25 time units.

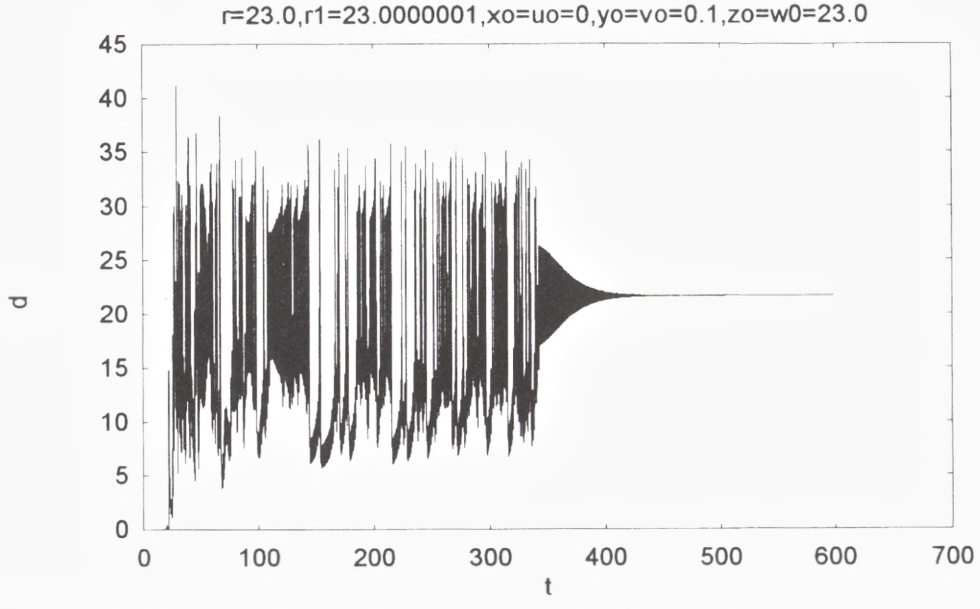

Fig. 6a: The stable part of the Lorenz attractor. Two integrations from the same initial states, but the forcing is changed by 10^{-7}. The two integrations arrive in different steady states.

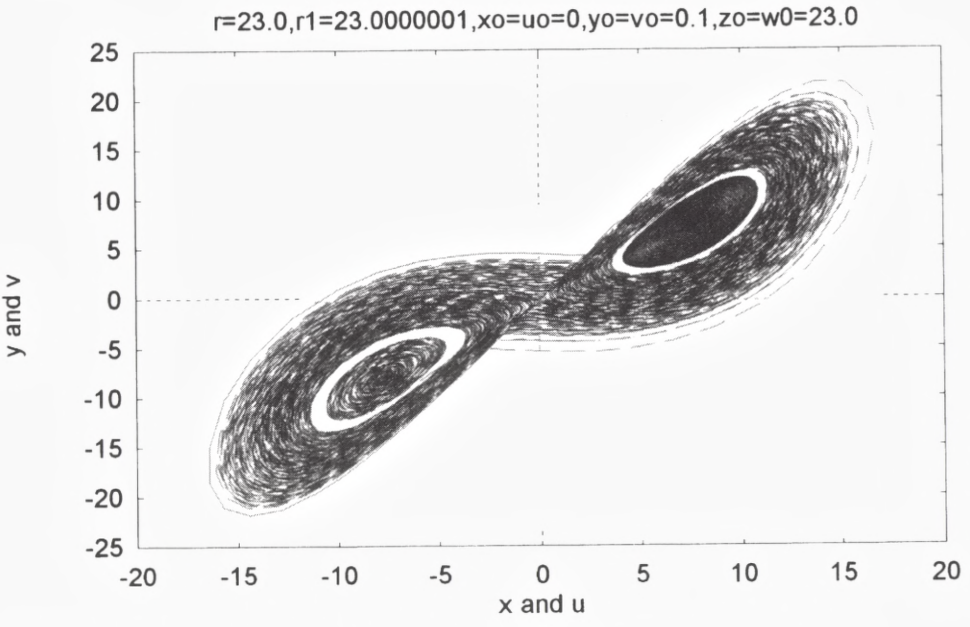

Fig. 6b: A plot of the (x,y) and the (u,v) trajectories for the integrations described in Figure 6a.

difference between two integrations, both starting in (0,0.1,23), but where one of the integrations have r=23, while the other has $r_1 = 23+10^{-7}$. Since the difference after more than 400 time units assumes a constant value, and since that value corresponds to the difference between the coordinates of the steady states, we can conclude that one of the two integrations finish in one of the stable steady states, while the other integration arrives in the other. Figure 6b containing the trajectories (x,y) and (u,v) shows clearly that the above statements are true. We notice also that each of the steady states is surrounded by a barrier. The two trajectories cross the barriers in this case.

Other initial conditions may lead to a different behavior. Figure 7a shows the difference between two integrations both starting in (1,0.1,23) with r=23 and $r_1 = 23 +10^{-7}$. Since the difference goes to zero and remains there after more than 400 time units, it is clear that in this case the two integrations have arrived in the same steady state. This statement is verified by Figure 7b showing that both integrations have reached the steady state located in the third quadrant. It should also be mentioned that none of the stable steady states may be reached for certain initial conditions. Figure 8a contains two trajectories with the common initial condition (0,0.1,23.7) and the same values of r and r_1 as in the previous examples. The regions around the stable steady states are empty, since it is impossible for any of the trajectories to

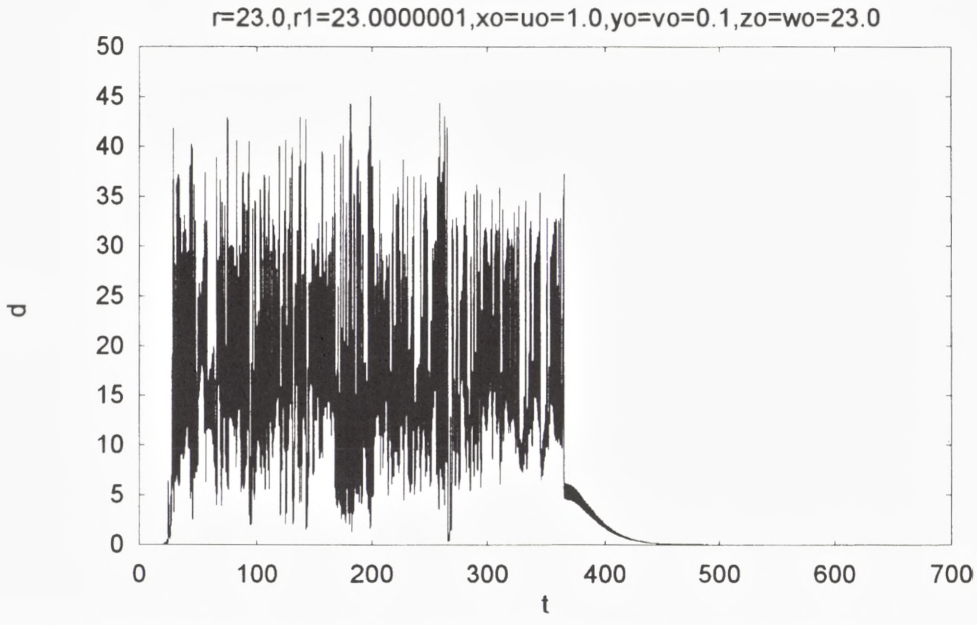

Fig. 7a: Corresponds to Figure 6a, but for a different initial state. The curve indicates that the two integrations arrive in the same steady state.

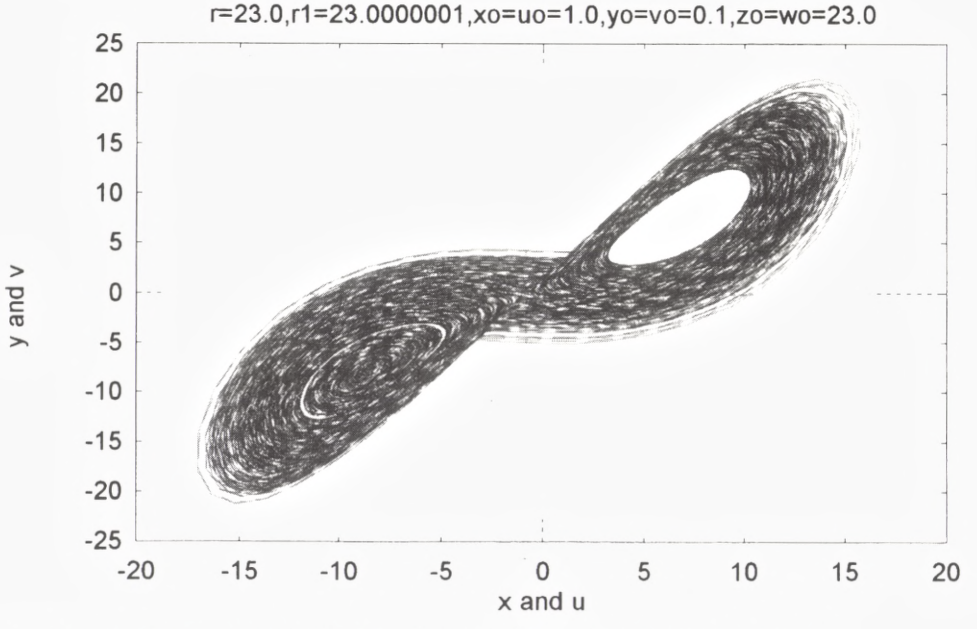

Fig. 7b: A plot of the (x,y) and (u,v) trajectories for the integrations described in Figure 7a.

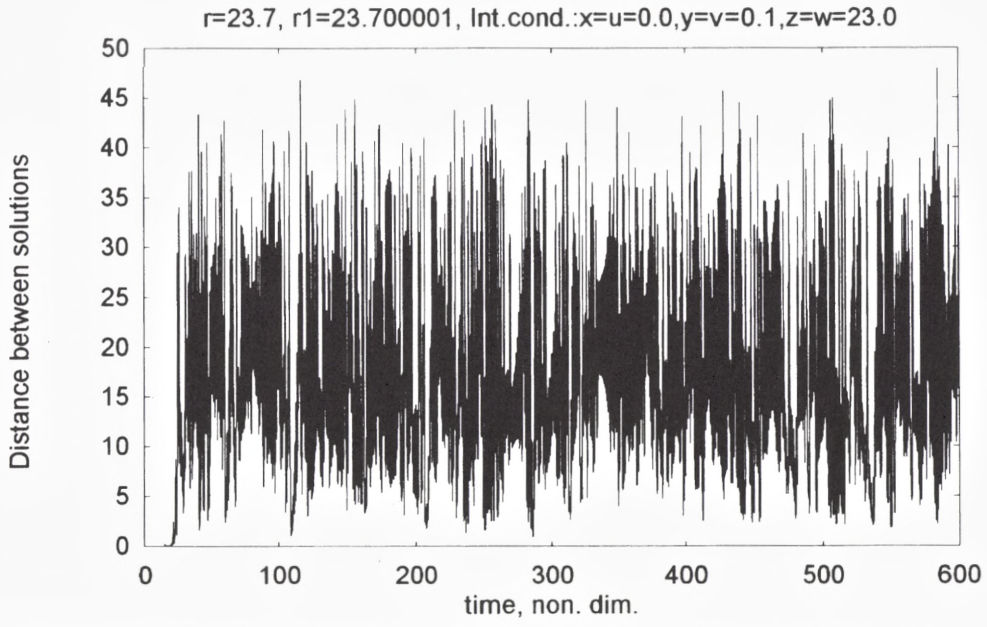

Fig. 8a: Corresponds to Figures 6a and 7a, but with the selected common initial state for the two integrations it is seen that none of them arrive in a steady state.

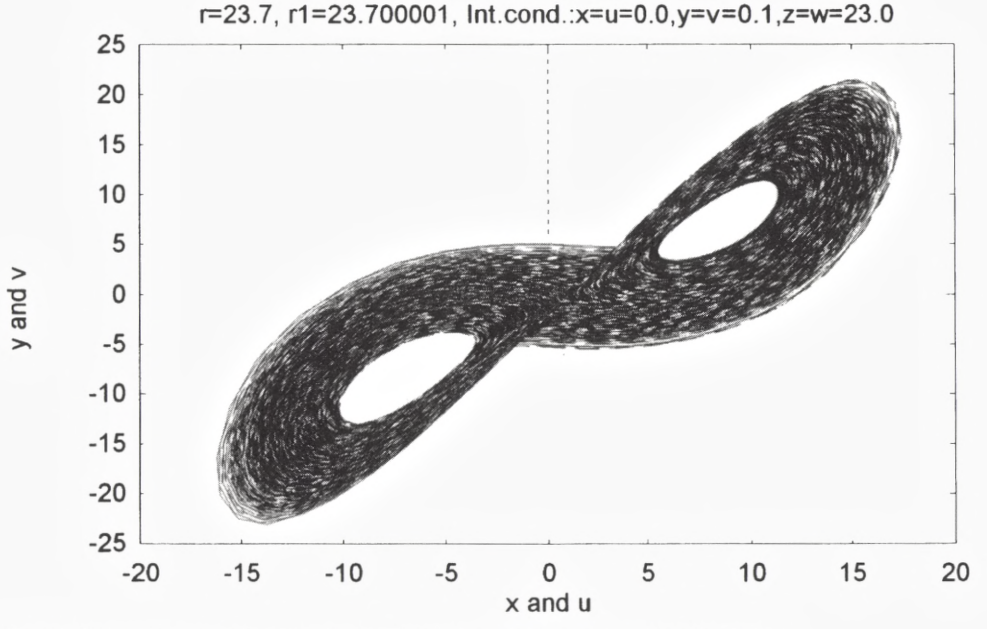

Fig. 8b: The trajectories of (x,y) and (u,v) for the integrations described in Figure 8a.

penetrate the barriers. Figure 8b shows the differences between solutions for the present case. It varies after the growth at about 20 time units.

Example B: Equation of motion with Newtonian forcing

As the second example we shall use a simplified form of the first equation of motion as given in (3.3).

$$\frac{\delta u}{\delta t} + u\frac{\delta u}{\delta x} = \gamma(u_E - u) \tag{3.3}$$

The equation is one dimensional in space. The right hand side contains a Newtonian forcing. It may be consider as a geopotential gradient field, constant in time, i.e. $\gamma\, u_E$, and a linear dissipation term. (3.3) is converted into the spectral domain by adopting the series given in (3.4).

$$\begin{aligned} u(t,x) &= \sum_{n=1}^{nmax} u(n,\, t)\, \sin\,(nkx) \\ u_E(x) &= \sum_{n=1}^{nmax} u_E(n)\, \sin\,(nkx) \end{aligned} \tag{3.4}$$

We have for simplicity selected the boundary conditions that u and u_E vanish at both boundaries. One could also have selected cosine-functions or a combination of both trigonometric functions. The series in (3.4) are inserted in (3.3) where the only nonlinear term is the advection term. The result is the equation given in (3.5).

$$\frac{du(n)}{dt} = {}^1\!/_2 \sum_{q=1}^{nmax-n} nku\,(q)\, u(n+q) - {}^1\!/_2 \sum_{q=1}^{n-1} qku(q)\, u(n-q) \tag{3.5}$$

The derivations necessary to come from (3.4) to (3.5) requiring the extensive use of Fourier expansions have been given by Wiin-Nielsen (1999). It is furthermore an advantage to non-dimensionalize (3.5). k is the basic wave number ($k=2\pi/L$) corresponding to the total length, L, of the interval. Introducing a scaling on time $T=\gamma^{-1}$ and on velocity $U=(2\gamma/k)$ we may write the basic equation in the form given in (3.6).

$$\frac{dx(n)}{d\tau} = \sum_{q=1}^{nmax-n} nx\,(q)\,x(n+q) - \sum_{q=1}^{n-1} qx(q)\,x(n-q) + x_E(n) - x(n) \qquad 3.6$$

(3.6) is general and can be used for specified values of nmax and $x_E(n)$. In a general case $x_E(n)$ should simulate the forcing at low wave numbers. Later in this section we shall use large values of nmax, but we shall first consider the most simple case with nmax=3. Renaming the variables x(1), x(2) and x(3) as x, y and z we find from (3.6) the three equations given in (3.7).

$$\begin{aligned} \frac{dx}{d\tau} &= xy+yz-x+x_E \\ \frac{dy}{d\tau} &= 2xz-x^2-y+y_E \\ \frac{dz}{d\tau} &= -3xy-z+z_E \end{aligned} \qquad (3.7)$$

The most simple case to analyse is x_E=0 and z_E=0. It is then easily found that the only steady state is (0,y_E,0), and that this steady state is unstable if y_E>2. However, values of y_E satisfying this inequality will not necessarily result in limited predictability. Values of y_E slightly larger than 2 lead to periodic solutions. Numerical experiments reveal that y_E>7.66 will lead to rather large differences between two solutions starting from the same initial conditions, but with differences in the forcing by 10^{-7}. For values of y_E<7.66 one obtains periodic solutions, but y_E>7.66 results in limited predictability. This can be seen from Figures 9a and 9b where the integrations have been carried out for 100 time units.

One may also use the system (3.6) with more components. In such a case it may be interesting to estimate the theoretical predictability. For this purpose the forcing was defined as seen in Figure 10a. The forcing, constant with respect to time, has a maximum of 20 units at wave number three and vanishes for n>10. The maximum wave number is 25. The forcing in the parallel experiment has the same form, but the maximum forcing is set to ($20\pm1\times10^{-8}$). Figure 10b shows the rms-difference between the two solutions. The difference vanishes for values less than 1.6. It may be reasonable to say that the predictability is lost when the rms-value exceed 1-2 m per s. We may therefore say that the limit of predictability is about 1.8 time units. To convert this non-dimensional value we recall that time is scaled by $\gamma^{-1}=10^6$ s. This value is of the correct order of magnitude, corresponding to a dissipation time

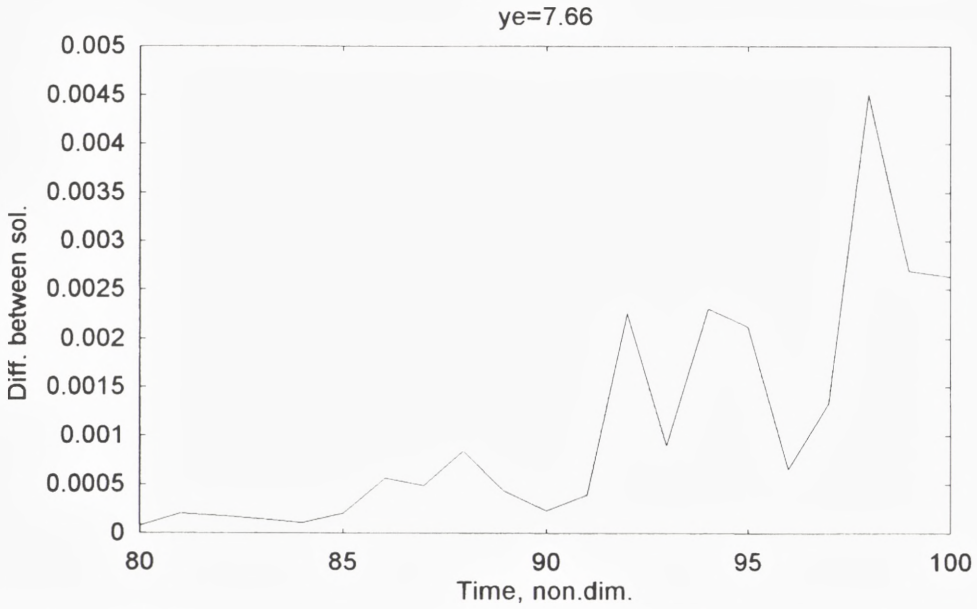

Fig. 9a: The RMS difference between two integrations of the three-component model based on the equation of motion for a value of the forcing of 7.66. Note the small values of the diference (less than 0.005).

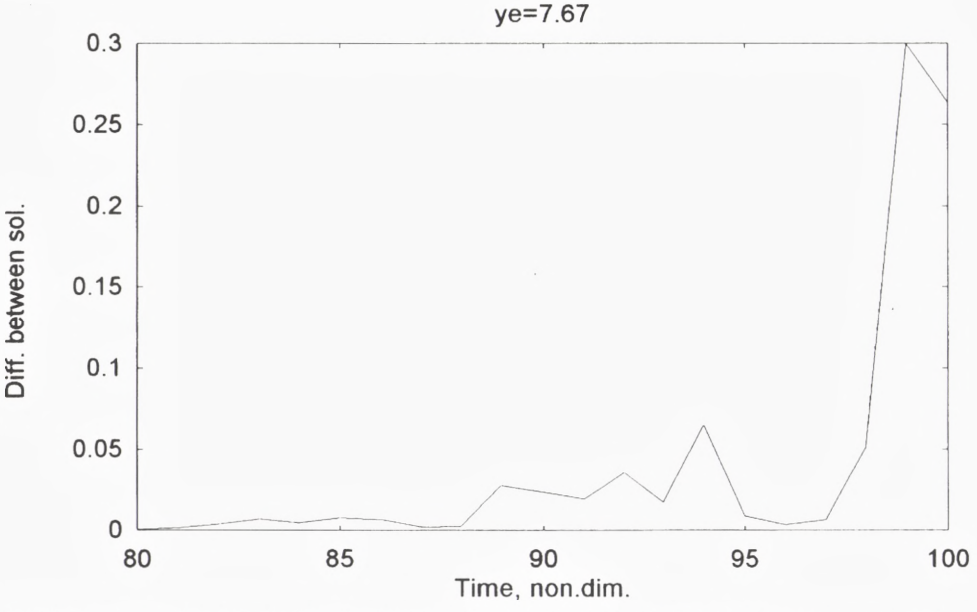

Fig. 9b: Corresponds to Fig. 9a, but the forcing is increased to 7.67. The RMS-difference is now much larger (up to 0.3).

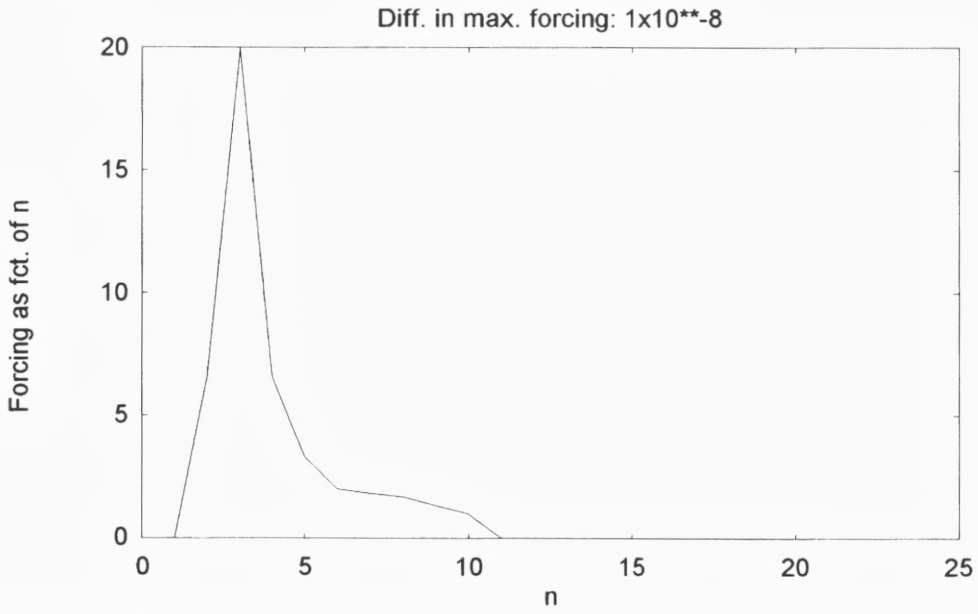

Fig. 10a: The forcing as a function of wave number for the experimental estimate of the theoretical limit of predictability.

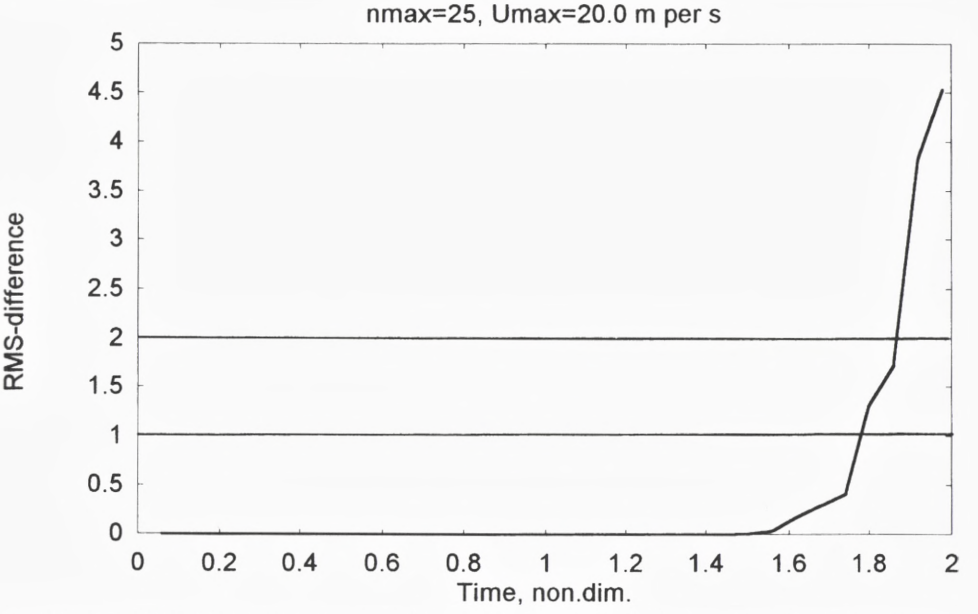

Fig. 10b: The RMS-difference between two integrations where the forcing is as in Fig. 10a for the first integration. In the second integration the forcing is changed by 10-8. The limit of theoretical predictability may be estimated to be 1.8 time units corresponding to 21 days.

of about 10 days, but one could also justify slightly smaller or larger values. Adopting the above value we find that the theoretical limit of predictability is about 21 days or 3 weeks. It corresponds to an extremely small change in the forcing, but assumes an accurate initial condition.

Example C: Wave-wave interaction

A model of wave-wave interaction on the sphere has been designed by Christensen and Wiin-Nielsen (1996) using interaction among the three longest planetary waves. This model was used to simulate blocking and the low-frequency oscillations described by Plaut and Vautard (1994). The monthly and intermonthly oscillations with periods of the order of magnitude of 70, 45 and 35 days was further investigated by Wiin-Nielsen (1996 and 1997) using a variety of models. The most advanced low-order model for these investigations is described in appendix 1 by Wiin-Nielsen (1997). For the purpose of the present investigation still another spherical model has been designed. The model is based on the barotropic vorticity equation with two components to describe the zonal flow and six spherical wave components. Since the latter components contain both sine and cosine components the total number of equations become 14. The model is with respect to the interac-

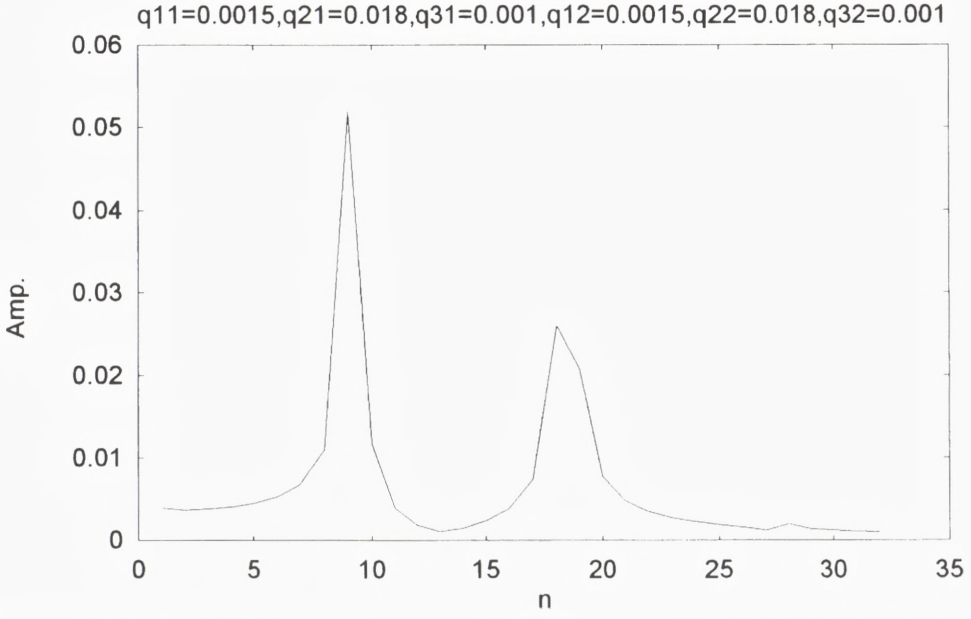

Fig. 11a: The amplitudes of the frequencies over a time interval of 630 days forced exclusively by wave forcing. The maxima at n=9 and n=18 correspond to periods of 70 and 35 days of atmospheric waves as determined from observational studies for selected time periods.

tions a special case of the general spectral barotropic model formulated by Platzman (1960). However, a forcing, constant in time, is added to each equation as well as a frictional term.

The model can simulate the monthly and intermonthly oscillations. To show this the model was integrated for a long time from an initial state of rest with forcing components on the waves of q11=0.0015, q21=0.018, q31=0.0001, q12=0.0015, q22=0.018 and q32=0.001. No forcing was applied to the two zonal components. These values of the forcing are the same in all integrations discussed in this case. A frequency analysis was performed for the last 630 days of the integration. Figure 11a shows the result. Maxima occur for n=9, corresponding to a period of 70 days, and for n=18, corresponding to a period of 35 days.

The experiment was repeated with an initial value on the two zonal components of only 0.001, while the initial values on all wave components remained at zero. Figure 11b shows the comparison between the two integrations. Maxima are still found at the same wave numbers, but the magnitude of the maxima are greatly reduced. The sensitivity to small changes in the initial state is still larger, when the initial values on the zonal components are changed to –0.001. Figure 11c shows that in this case we have large changes as compared to Figure 11a. These results in-

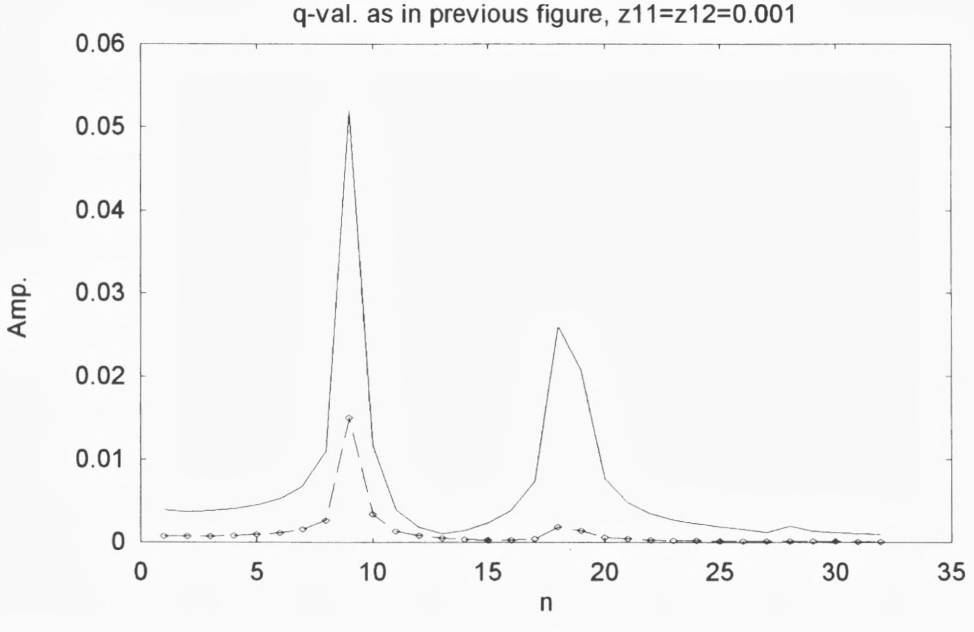

Fig. 11b: The amplitudes from Figure 11a (solid) and the amplitudes (dashed) when initial values of the zonal components of 0.001 is used.

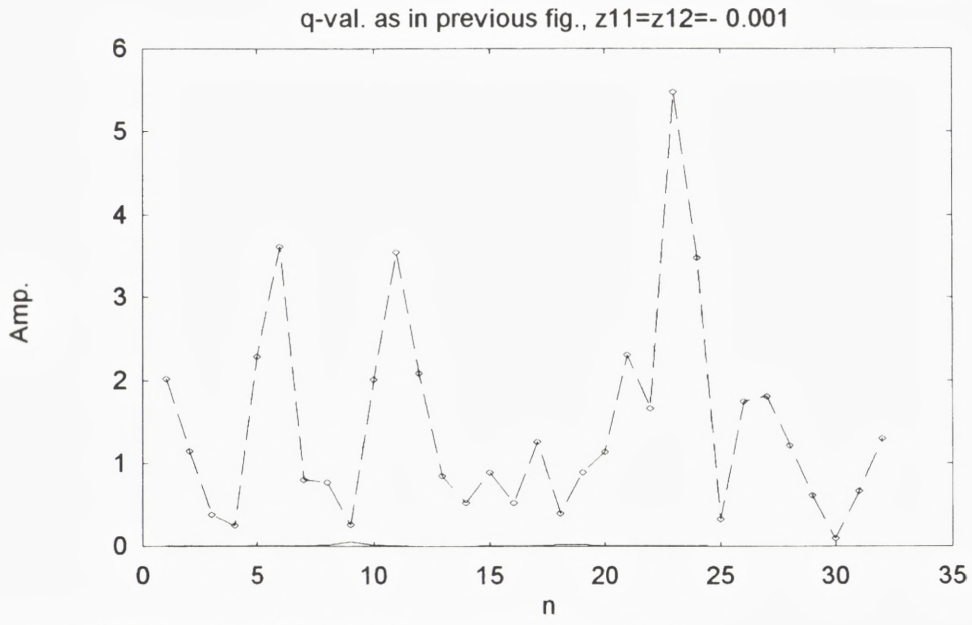

Fig. 11c: The frequencies, when the initial zonal components are – 0.001.

dicate that the occasional periodic motion observed in the atmosphere is due to a dominating abnormal eddy heating generating the quasi-periodic oscillations.

Example D: Barotropic model

The low-order model is formulated on the beta-plane. It has 2 components, z_1 and z_3, describing the zonal flow, and 4 components, x_1, y_1, x_3 and y_3, describing the eddies. The model, its equations, the stability properties and some integrations have been described by Wiin-Nielsen (1961). The dependent variables are scaled in such a way that all of them have the dimension: m per s. The model can simulate the nonlinear aspects of barotropic instability, and it contains a eddy momentum transport that interacts with the zonal current. We shall in the present section show the sensitivity of the model to small changes in the initial state. For this purpose we have selected a length of the channel of 5000 km and a width of 6000 km. The initial state has $z_1 = 30$ m per s, $z_3 = -15$ m per s and $x_1 = 7.5$ m per s. The other components are zero initially. In the second integrations the zonal components are changed by 2% to the values: 30.6 and –15.3 m per s. The eddy component x_1 is shown in Figure 12a for the two integrations in the time interval from 10 to 20 days as seen on the abscissa. It is seen that the separation between the two integrations is starting. Figure 12b shows the same two curves, but for the time interval from 90 to

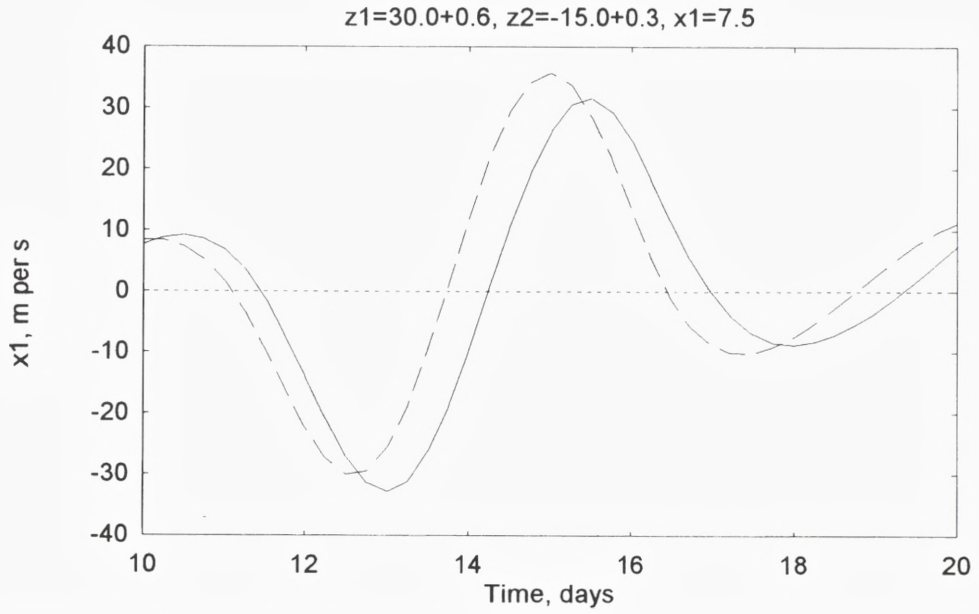

Fig. 12a: The difference for the time interval from 10 to 20 days between two integrations in which the initial zonal values are changed by 2%.

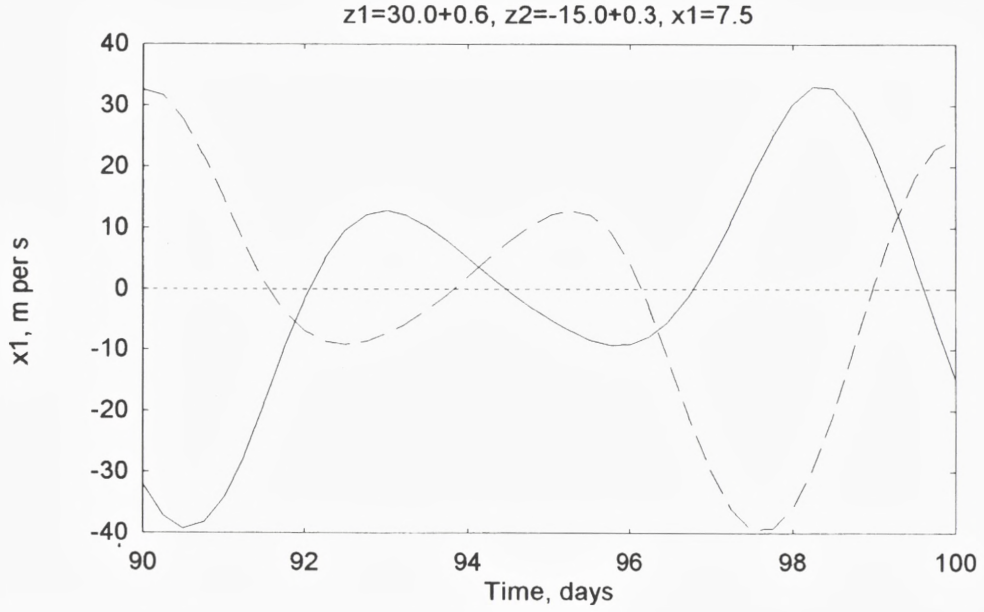

Fig. 12b: As Fig. 12 a, but for the time interval from 90 to 100 days.

100 days. The integrations show a similar separation of all the other dependent variables, including the momentum transport. We have thus used the barotropic model as an example of limited predictability. The two long integrations indicate that transient waves will gradually show very different phases of the waves in the two integrations.

Example E: Baroclinic model with heat transport only

Simple low order, two level, nonlinear baroclinic models have been designed by the author (Wiin-Nielsen, 1991, 1992). They contain a zonal current, but only one wave component, satisfying the boundary conditions at the southern and northern walls on the beta-plane. With two components describing the zonal flow and sine and cosine components to describe the eddies at the upper and lower levels we obtain a model with six components. Since only one meridional wave is present, these models will not have momentum transports by the waves, but a transport of sensible heat will take place. Another implication of this choice is that the vertical mean zonal current will be influenced only by dissipation and thus go to zero during a long integration. We will therefore have to focus on the thermal processes. The model contains a specified zonal and eddy heating and dissipative mechanisms in the usual parameterizations.

The case to be considered in this example will contain a zonal heating with a maximum of 4.0×10^{-3} W per kg, but no eddy heating. It corresponds thus to the type of experiment carried out by Phillips (1956). The initial state is a state of rest except for very small values of 0.001 on the eddy components. The heating will gradually create a meridional temperature difference with low temperatures to the north and high temperatures to the south, and when the temperature gradient has become sufficiently large baroclinic instability will create a growing wave. When the amplitude of the wave becomes large the nonlinear aspects of the model will start to act. This will happen with the present parameters after about 50 days. We shall select the eddy transport of heat to show the effect of the limited predictability. The two integrations to be compared differ only in zonal heating which in the second integration was changed to 4.04×10^{-3} W per kg corresponding to a change of 2%.

Figure 13 shows the maximum transport of sensible heat during the time interval from 90 to 100 days. It is seen that a significant difference between the two integration has taken place. This statement applies also to all the other dependent variables.

Example F: Baroclinic model with heat- and momentum transport

As the final example of a meteorological nature we select still another low order model containing 12 components, 6 at each of the two levels in the model, which

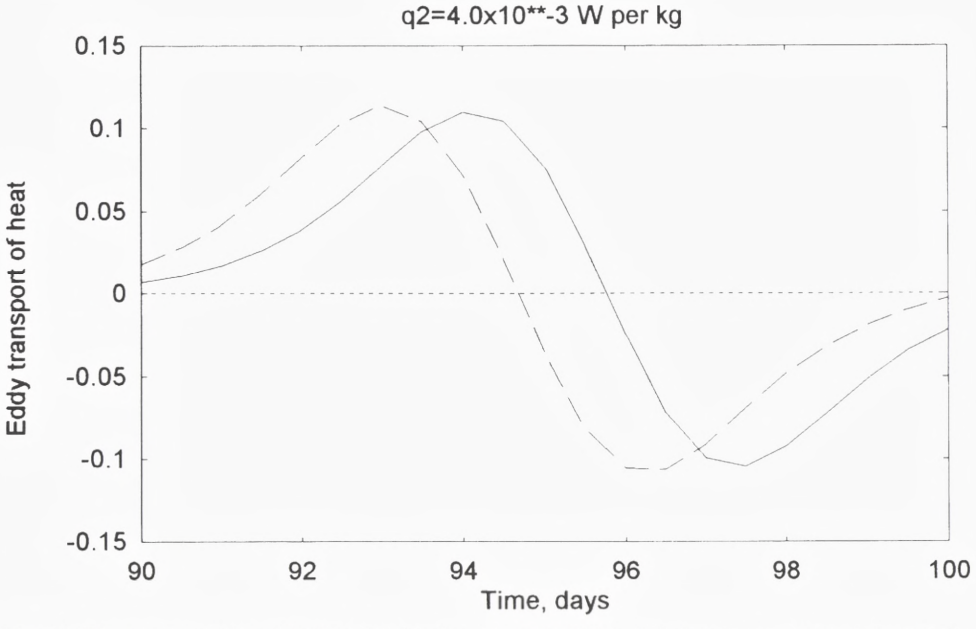

Fig. 13: The transport of sensible heat for the time interval of 90 to 100 days for a change of the zonal forcing by 2%. Note that the difference for the minima is almost 2 days.

has the same components at each level as the barotropic model had at a single level. Two variables with wave numbers 2 and 4 describe the zonal flow at each level. Four variables at each level with meridional wave numbers 1 and 3 describe the waves at each level. The waves have the same wavelength equal to the length of the channel. The model is forced by a heating function that has the same wave structure as the variables, i.e. zonal and wave heating. The dissipation is included as boundary layer friction and internal friction proportional to the vertical shear flow. The two meridional scales are the minimum for a non-zero momentum transport. The model has been described and used in many ways by Marcussen and Wiin-Nielsen (1999). We shall add a single example illustrating limited predictability.

The forcing is restricted to heating in the south-north direction. The initial conditions is a state of rest except for very small values (1 mm per s) of the eddy components. The model will create a temperature difference between the south and the north resulting eventually in barotropic-baroclinic instability. The waves will increase in amplitude and eddy transports of sensible heat and momentum will gradually increase.

Two integrations are performed with heating on the meridional wave with wave number 2 of $2x10^{-3}$ W per kg in one integration and $2.02x10^{-3}$ W per kg in the oth-

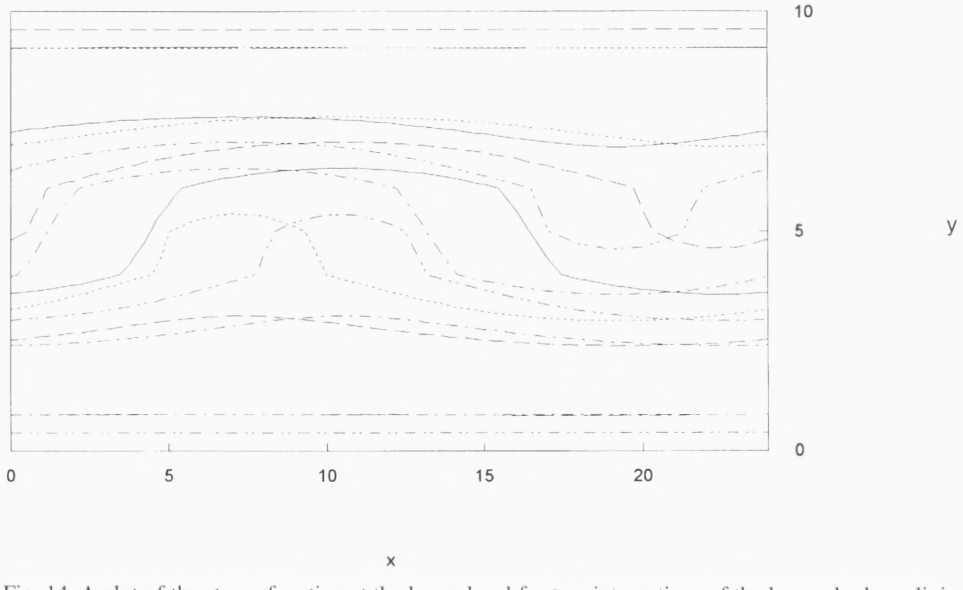

Fig. 14: A plot of the streamfunction at the lower level for two integrations of the low order baroclinic model with transports of both heat and momentum.

er. The width of the channel is 6000 km and the selected wavelength in the west-east direction is 4000 km. Figure 14 shows the streamfunctions at the lower level (750 hPa) for the two integrations, when the waves have reached the largest amplitudes. The difference between the two states is quite large indicating the limited predictability.

Example G. The magnetic field of the Earth

A simple and schematically correct model of the magnetic field of the Earth may be developed by simulating the magnetic field by a dynamo. The magnetic field of the Earth has reversed its direction repeatedly. Such reversals take place in an irregular manner, and they seem to happen on average every 340000 years. Between reversals the magnetic field fluctuates irregularly. The reversals take place rapidly compared to the average time between reversals. A single reversal takes only a few thousand years.

A behavior of the type described above may be simulated by considering an experiment as shown schematically in Figure 15. We have two vertical axes. A disc rotates around each vertical axis. A conducting coil is connected to each axel and to the periphery of each disc. Each coil has a circuit taking it from the axel around the

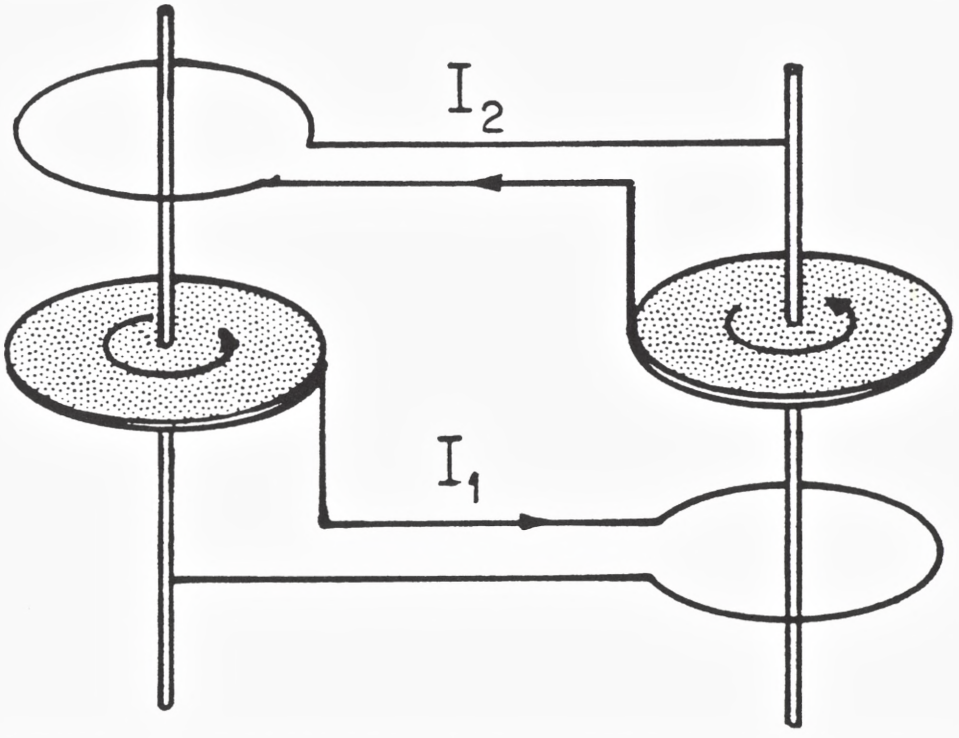

Fig. 15: The current goes in each case from the disc around one of the vertical axes and back to the other.

other axel and back to the periphery of the disc. The rotation of the discs start with a certain velocity by applying a constant torque to the axel in order to turn the discs. The arrangement of the circuits will introduce magnetic fields which will interact with the magnetic field created by the rotation.

The important parameters of the experiment are the speed of rotation of each disc, the moments of inertia of the discs, the resistances in the circuits, the self-inductances and the voltages. A detailed discussion of the derivation of the proper equations is given by Beltrami (1987) and will not be repeated here. The equations are made nondimensional with the nondimensional time τ and the three dependent variables x, y and z of which x and y are the nondimensional currents, corresponding to I_1 and I_2 on Figure 15, while z is the nondimensional angular velocity of one of the discs. The angular velocity of the other disc is $z\text{-}\gamma$. μ is a nondimensional constant. The equations are finally as given in (3.8).

$$\frac{dx}{d\tau} = yz - \mu x$$

$$\frac{dy}{d\tau} = x(z-\gamma) - \mu y \tag{3.8}$$

$$\frac{dz}{d\tau} = 1 - xy$$

The equations have two steady states, which may be written as given in (3.9).

$$\bar{z} = {}^1/_2[\gamma + (\gamma^2 + 4\mu^2)^{1/2}$$

$$\bar{x} = \pm \left(\frac{\bar{z}}{\mu}\right)^{1/2} \tag{3.9}$$

$$\bar{y} = \pm \left(\frac{\bar{z}-\gamma}{\mu}\right)^{1/2}$$

In (3.9) we have only one value of the third variable because the angular velocity is defined as a positive quantity. The stability of the two steady states may be determined by solving the cubic frequency equation for the linearized version of the three equations given in (3.8). The result is that they are always unstable. We have therefore a situation which is very similar to the Lorenz-equations in the unstable case considered earlier in this paper.

Figure 16a shows the trajectory of (x,y) for an integration over 500 time units. The integration is carried out when both γ and μ are equal to 1. The two dots indicate the position of the unstable steady states. It is seen that the trajectory for some time goes around one of the steady states whereafter it changes to go around the other steady state.

Also in this case we have investigated the limited predictability. The two integrations were carried out for identical initial states, while the values of γ and μ were changes by 10^{-8}. Figure 16b contains the RMS-difference between two solutions. The difference starts to grow at about 120 time units whereafter it varies in an irregular way.

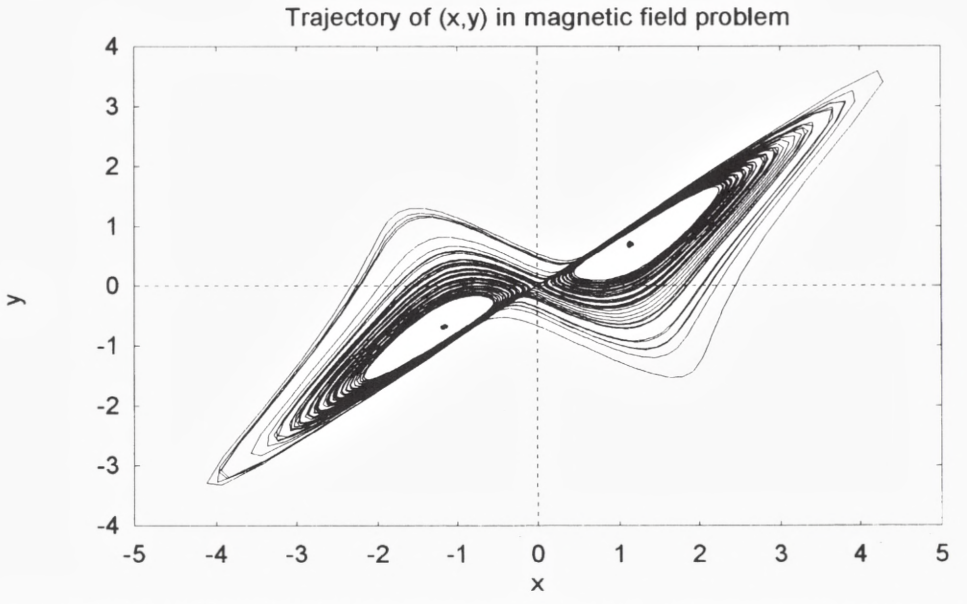

Fig. 16a: The two dots indicate the position of the steady state in the xy-plane. The trajectory of (x,y) goes several times around one of the steady states whereafter it changes to a similar behavior with respect to the other steady state.

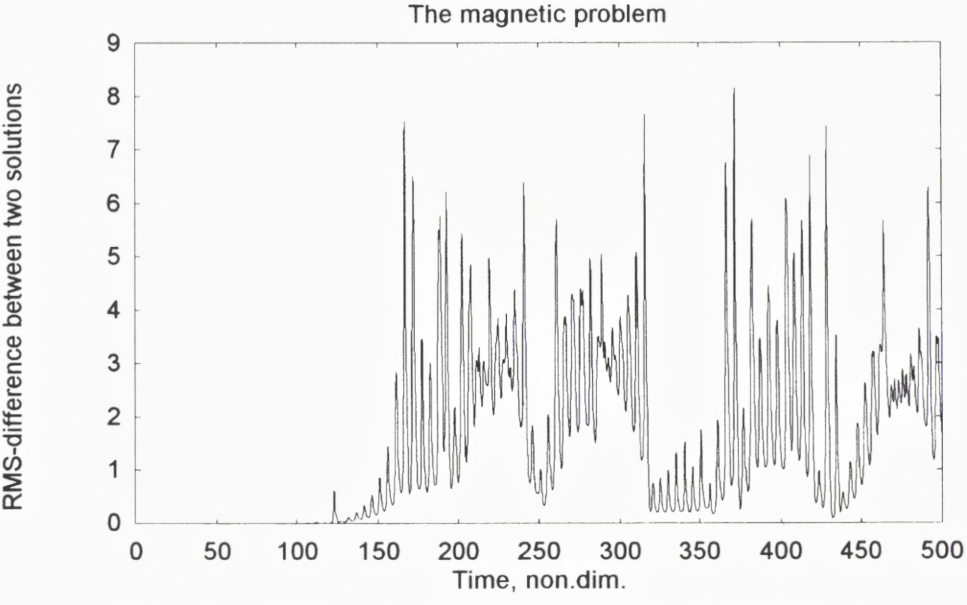

Figure 16b: The limited predictability of the system is clearly indicated by the RMS-difference between the two integrations.

4. Limited predictability and the uncertainty of parameters

The examples given above contain in most cases several physical parameters as well as the numbers defining the initial state. To find the sensitivity to changes in these numbers we deal with a multidimensional space. It may therefore be an advantage to use particularly simple models to investigate how the predictability depends on the uncertainty of for example a single parameter. As the first case we shall select the so-called Feigenbaum (1978) problem because it is especially simple, and because it has played an important rôle in the first investigations of chaos.

The Feigenbaum problem is governed by the equation in (4.1) in which K is the so-called carrying capacity. We note that N(n)=K is a steady state.

$$N(n+1) = aN(n)\,[1-N(n)\,/\,K] \tag{4.1}$$

We may scale N(n) by K, i.e. N(n)=K x(n), and the equation takes then the form given in (4.2).

$$x(n+1) = ax(n)\,[1-x(n)] \tag{4.2}$$

The interpretation of the equation may be given in terms of the growth or decay of a single population living in isolation from all other populations. The number of members in the new generation, x(n+1), depends on the birth and death rates of the present generation where the first process is calculated by the first term ax(n), while second process is simulated by $ax(n)^2$. The equation in the form (4.1) has been nondimensionalized in such a way that the number of individuals in the n'th generation will be between 0 and 1.

It is well known that the solution becomes chaotic when the value of a exceeds the Feigenbaum number. In the following integrations we have selected the basic a to be 3.7. We compare integrations starting from a common initial state (0.5) and with values of a increasing by addition of 10^{-2}, 10^{-3},..10^{-8}.

For each pair of integrations we will after a while notice a divergence of the two solutions. The step at which the difference between the two solutions become different from zero and thereafter increases significanly has been noted. Table 1 contains the step at which the difference between the two solutions starts to increase significantly.

Table 1

a	10^{-2}	10^{-3}	10^{-4}	10^{-5}	10^{-6}	10^{-7}	10^{-8}	10^{-9}
step	1	5	11	20	36	38	39	40

For the basic value of a=3.7 we find that the predictability increases from the first step to about step 40.

As the next example we select the model using the first equation of motion in one space dimension and driven by a Newtonian forcing, see eq. (3.3) and the following equations. We use as in the previous case a maximum value of u_E of 20.0 and the same distribution of the forcing as a function of the wave number. The experiment is then to compare integrations where the maximal value of u_E is increased by the same powers of 10 as given in Table 1. Using the nondimensional form of the equation we have to convert the results to a predictability time in f. ex. the unit of days. Table 2 contains the results.

Table 2

u_{Em}	10^{-2}	10^{-3}	10^{-4}	10^{-5}	10^{-6}	10^{-7}	10^{-8}	10^{-9}
Pr. T days	9.3	11.6	12.7	13.9	15.0	17.4	18.5	20

We know from the previous investigation of the same basic equation that our estimate of the theoretical predictability is close to 21 days. Table 2 shows that in our example we need to know the forcing with extreme accuracy in order to attain the theoretical limit of predictability. To the extent that our example using a simple equation in one space dimension and with a forcing independent of time is valid at least with respect to the order of magnitude it indicates how difficult it is to come close to the theoretical limit.

As the next example we select the case of competition among three species. Several special cases have been treated by May (1976) and Beltrami (1987). We select here the general case with full interactions. The following equations have been nondimensionalized as found in the above references. They take the form given in (4.3).

$$\begin{aligned} \frac{dx}{dt} &= x(1-x-ay-bz) - cyz \\ \frac{dy}{dt} &= y(1-y-az-bx) - cxz \\ \frac{dz}{dt} &= z(1-z-ax-by) - cxy \end{aligned} \tag{4.3}$$

These equations have a steady state where the three coordinates are equal to each other as given in (4.4).

$$\bar{x}=\bar{y}=\bar{z}=\frac{1}{1+a+b+c} \tag{4.4}$$

No other steady states have been found. A stability analysis can be carried out in the usual wave by linearization around the steady state. The results of the stability analysis gives three values of the frequencies. They are given in (4.5).

$$\begin{aligned} \nu_1&=-1 \\ \nu_{2,3}&=-\bar{x}(1-2c-{}^1/_2(a+b)\pm{}^1/_2 i 3^{1/2}(a-b)) \end{aligned} \tag{4.5}$$

It is thus seen that the steady state will be stable if c satisfies the inequality given in (4.6).

$$c<{}^1/_2(1-{}^1/_2(a+b)) \tag{4.6}$$

The result in (4.6) has been tested and verified by numerical integrations where the initial values of x, y and z are equal. However, if an arbitrary initial state is used, it turns out that smaller values of c are needed, if the integration shall arrive in the stable steady state.

A single example will be shown. Two parallel integrations were performed with a common initial state (0.9,0.7,0.3). In one of the integrations a, b and c have the values 0.6, 0.7 and 0.102, while the values 0.61, 0.69 and 0.092 were used in the other. Since the steady states are stable, the two integrations should reached these steady state asymptotically. Figure 17, showing the RMS-difference between the two integrations, shows that both of them arrive in the proper steady state. However, due to the difference in the values of the parameters the RMS values increase initially and reach rather large values after an integration time of about 30 units. In this case of stable steady states we have only limited predictability in the short time range.

The pendulum is a classical example of a nonlinear system. We consider a pendulum consisting of a slim, rigid and massless rod of length l connected to a pivot and ending in a bob of mass m. The pivot is made in such a way that the pendulum can move in a plane only. The forces working on the pendulum are gravity and the friction from the air. Two steady states can be found. The first is the position where the bob is in the lowest position. This steady state is stable as we all know. The second stationary position is the case where the bob is in its highest position. A small

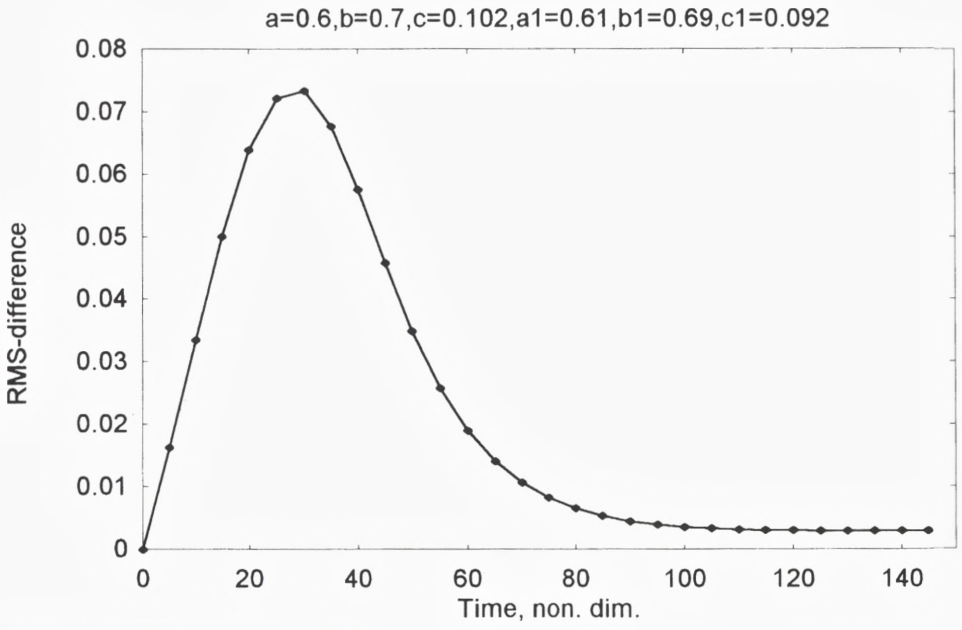

Figure 17: The RMS-difference between two solutions for a common initial state, but slightly different values of the parameters a, b and c.

deviation from this position will give the pendulum a violent oscillation, but due to the friction it will eventually end in the stable state, where the bob is in the lowest position.

The equation for the movement of the bob is derived in elementary textbooks of physics. The angle θ is zero when the pendulum is at rest and measures in general the deviation from the resting position. The general equation for the movement of the pendulum is derived from Newton's law saying that mass times acceleration is equal to the sum of the forced acting on the system. We get then the following equation:

$$\frac{d^2\theta}{dt^2} = -r\frac{d\theta}{dt} - \frac{g}{l}\sin(\theta) \tag{16}$$

where r is the coefficient for the frictional force and g is gravity. Eq. (16) is nonlinear due to the trigonometric term. It cannot be solved by analytical means. If one restrict the motion to small angles from the resting position, one may replace $\sin(\theta)$ by θ in which case the equation becomes an ordinary differential equation of the second order, and the solution can be obtained by elementary means. Another sim-

ple case is the one where it has been assumed that the frictional term may be neglected. In the general case the equation have to be treated by numerical integration. It is an advantage to replace the single equation by two equations. We define $x=\theta$ and $y=d\theta/dt$. x may be named the position of the bob, while y is the angular velocity. We get then the following equations:

$$\frac{dx}{dt} = y$$
$$\frac{dy}{dt} = -ry - \frac{g}{l} \sin(x) \tag{17}$$

We may be sure that the gravity g is known with excellent accuracy. The same should be the case for length l of the rod. However, the coefficient representing the friction included in the model is known with far less accuracy. The initial state is given by the value x_o, measuring the initial angle from the vertical position, where the bob is in the lowest position, and the initial angular velocity y_o, which in the

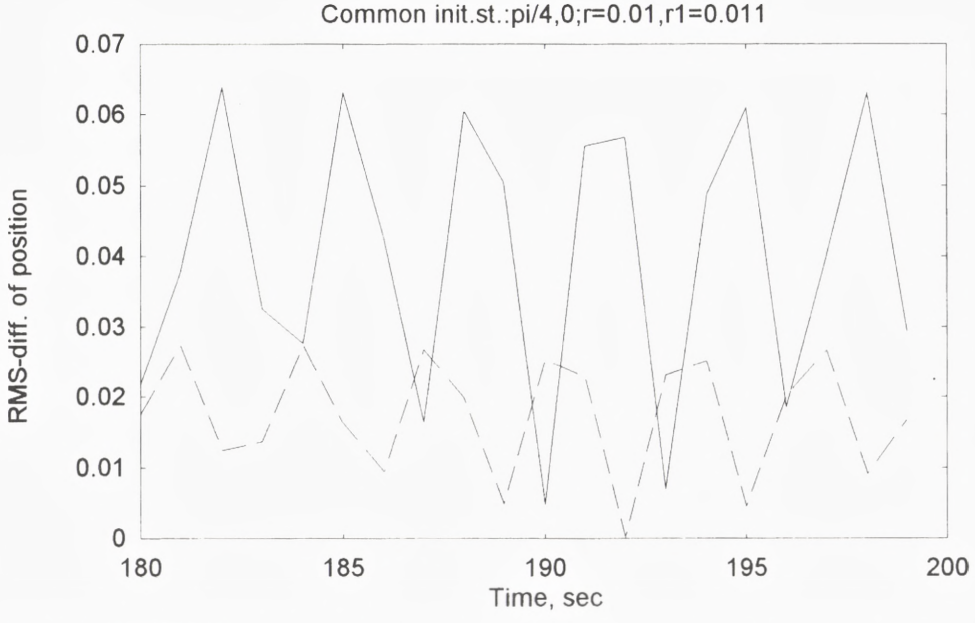

Figure 18: The RMS-difference of the position as a function of time for the pendulum problem. The two curves compare the differences for the general case and the linearized equation for the same initial condition, but with values of the frictional parameter being 0.01 and 0.011.

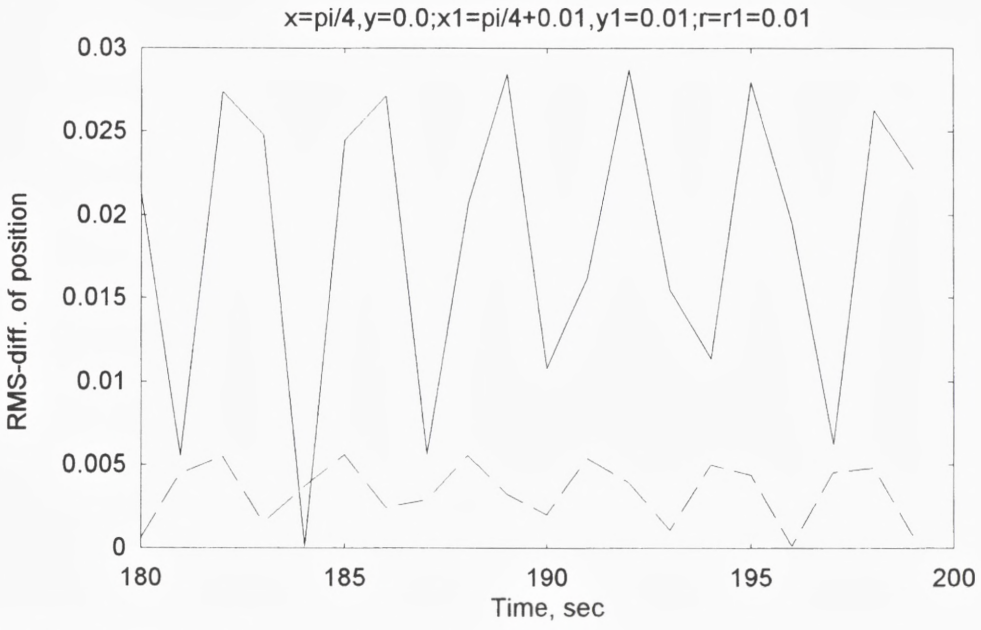

Figure 19: Similar to Figure 18, but with identical physical parameters, but small changes in the initial state as given above the figure.

present case is chosen to be zero. One may assume that these values can be given with good accuracy. The only large uncertainty in the problem is therefore the value of the frictional coefficient.

In the following we shall compare numerical solutions of the general case and the case where the sine functions has been replaced by the angle measured in radians. Figure 18 shows the RMS-differences of the position (x) between two solutions of the general case with r=0.01 and r_1=0.011, while the other curve is the same RMS-difference for the special, linear case. It is observed that the general nonlinear case has much larger RMS-differences than the linear case. We may also give the sensitivity to small changes in the initial state. Figure 19 contains a comparison between two cases with the same physical parameters, but the initial state has been changed by adding 0.01 to both the angular position and to the initial angular velocity. Again we notice that the linear case has much smaller RMS-values than the nonlinear case. This case does not fall in the class of chaotic flows since it has a well defined asymptotic state of rest. The examples show only that two different values of the friction parameter implies two different paths to the steady state.

5. Summary and concluding remarks

The purpose of the present paper is to discuss the limited predictability of nonlinear systems. The weather predictions using atmospheric models have been selected in Section 2 to illustrate limited predictability in a well documented geophysical field with experience covering half a century. Section 3 contains a number of low order atmospheric models used to illustrate the main aspects of sensitivity to small changes in the initial state or the forcing of the system. Section 3 contains also an attempt to estimate the theoretical limit of predictability.

During the last century we have gradually learned and tested that almost all nonlinear systems show limited predictability. The nonlinear equations that can be solved in a closed mathematical form are very few and very simple. The original optimistic view that valid predictions could be made for unlimited times if the initial state and the forcing were known with excellent accuracy has been replaced with a much more realistic view, because we in most cases by numerical experiments can determine the operational limits of predictability, or, in other words, we have a better understanding of what we can and cannot do. At the same time it has to be realized that this view have not so far been accepted by all groups engaged in predictions of climate change and social and economical affairs.

Regarding the application of predictions it should be pointed out that predictions for a week or so do not permit any possibilities to influence the validity of the predictions. The weather forecasts are valid for such a short time that anthropogenic influences are negligible on this time scale. On the other hand, predictions of the second kind for extended periods such as predictions of climate change or predictions of an economic or social nature can indeed be counteracted by measures or activities that will influence the validity of the forecast. As a matter of fact, the production of economic forecasts is used by governments and institution to produce counter-measures that should decrease the impact of unwanted predicted developments. Another example is the attempted simulations of the future climate changes created by anthropogenic influences on the climate. We shall as a matter of fact never have the possibility to verify the validity of these simulations when measures are taken by governments and large institutions to decrease the anthropogenic influences.

Other fields that have been investigated in some detail are competition among three or more species (May and Leonard, 1975, May, 1976, Beltrami, 1987, Wiin-Nielsen, 1998) and population dynamics (Feigenbaum, 1978), but many other areas still need to perform all the numerical experimentation necessary to determine the behavior of the prediction procedures in their field.

5. Acknowledgement

The author would like to express his appreciation to Dr. D. Burridge, the Director of the European Centre for Medium-Range Weather Forecasts, for providing information on operational predictability and its development over the last few years.

Appendix 1

The purpose of this appendix is to give an example of limited prediction in the classical three body problem which gave the first example on limited predictability. The equations for the problem are well known and can be found in any book on theoretical astronomy. We denote the masses of the three bodies by m, m_1 and m_2, the position vectors by **r**, $\mathbf{r}_1$ and $\mathbf{r}_2$, the velocities by **v**, $\mathbf{v}_1$ and $\mathbf{v}_2$, and the distances between the three bodies by r_{o1}, r_{o2} and r_{12}. The universal gravitational coefficient is denoted by μ. The vector equations of motion are then given in (A1).

$$\begin{aligned}
\frac{dv}{dt} &= \mu m_1 \frac{r_1 - r}{r_{o1}^3} + \mu m_2 \frac{r_2 - r}{r_{o1}^3} \\
\frac{dv_1}{dt} &= \mu m \frac{r_1 - r}{r_{o1}^3} + \mu m_2 \frac{r_2 - r_1}{r_{12}^3} \qquad \text{(A1)} \\
\frac{dv_2}{dt} &= \mu m \frac{r_2 - r}{r_{o2}^3} + \mu m_2 \frac{r_2 - r_1}{r_{12}^3}
\end{aligned}$$

The remaining three equations are simply the definition of the vector velocities as seen from (A2).

$$\begin{aligned}
\frac{dr}{dt} &= v \\
\frac{dr_1}{dt} &= v_1 \qquad \text{(A2)} \\
\frac{dr_2}{dt} &= v_2
\end{aligned}$$

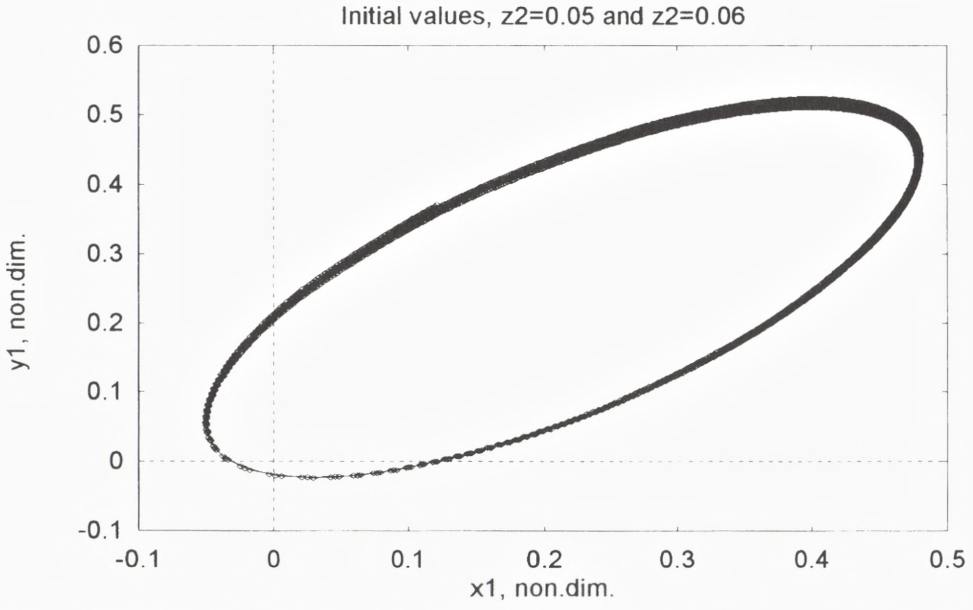

Fig. A1: The trajectories of (x1,y1) in the three-body problem when the initial values of z2 is changed from 0.05 to 0.06.

We have thus 6 first order vector equations. Since each of the vectors have three components we obtain 18 first order scalar equations. These equations are obtained in a non-dimensional form by selecting a standard mass M and writing the masses as $m = cM$, $m_1 = c_1 M$ and $m_2 = c_2 M$. Thereafter we introduce a length scale a and a time scale T and select these in such a way that $\mu M T^2 / a^3 = 1$. The effect of the scaling is that μm becomes c, μm_1 becomes c_1 and μm_2 becomes c_2 in equations (A1), while (A2) can be wrtten in the same form.

The resulting 18 scalar equations have been integrated numerically using the Heun scheme. The following case will be illustrated: $c=10$, $c_1=10^{-3}$, $c_2= 10^{-6}$, and the following initial values $x_1=0.4$, $y_1=0.5$, $z_1=0.6$, $x_2=0.25$, $y_2=0.3$, $z_2=0.05$, $u_1=u_2=1$, $w_1=0.2$, $w_2=0.3$, while the remaining initial values of position and velocity were selected to be zero. Two integrations were carried out. The first integration had the initial values stated above, while the second integration had $z_2 = 0.06$. Figure A1 shows as an example that the predictions for x_1 and y_1 were changed only slightly. The same result is obtained when figures are made of the trajectories of (x_1,z_1) or (y_1,z_1). Figure A2 shows z_2 as a function of time for the interval $1<t<3$. It is seen that the two curves have differences in the amplitudes and also a steadily increasing phase difference. A small change in the initial value results thus in large differences at a later time. We have thus an example of limited predictability.

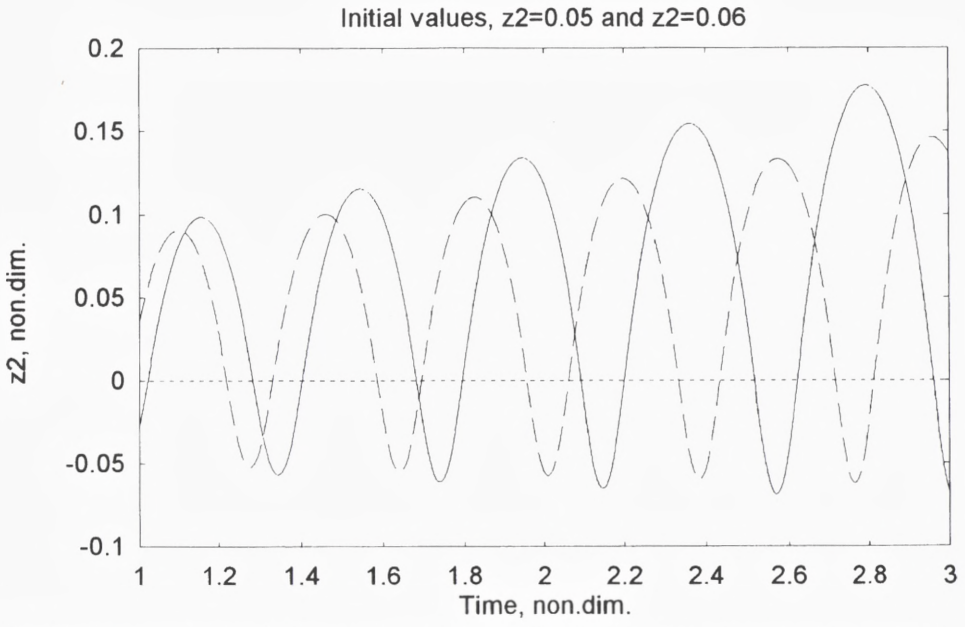

Fig. A2: The component z2 for the two integrations described in Fig. A1 as a function of the nondimensional time for 3 time units. It is seen that the two integrations gradually come out of phase.

References

Beltrami, E., 1987: Mathematic for dynamic modeling, Acad. Press, 277 pp.

Bengtsson, L, 1985: Medium-Range Forecasts - the experience at ECMWF, GARP special report,, No. 43, World Meteorological Organization,, 113-132.

Charney, J.G., 1966: The feasability of a global observation and analysis experiment, Nat. Acad. of Sci., Res. Council, 172 pp.

Christensen, C.W. and A. Wiin-Nielsen, 1996: Blocking as a wave-wave interaction, Tellus, 48A, 254-271.

Feigenbaum, M., 1978: Quantitative universality for a class of nonlinear equations, Jour. of Stat. Physics, 19, 25-52.

Lin, H. and J.F. Derome, 1995: On the thermal interaction between the synoptic-scale eddies and the intra-seasonal fluctuations in the atmosphere, Atmos.-Ocean., 33, 81-107.

Lorenz, E.N., 1963: Deterministic nonperiodic flow, Jour. of Atm.Sci., 20, 130-144.

Lorenz, E.N.,, 1993: The essence of chaos, Univ. of Washington Press, 226 pp.

Marcussen, P. and A. Wiin-Nielsen, 1999: A numerical investigation of a simple spectral atmospheric model, Atmósfera, 12, 1, 43-73.

Mason, B.J., 1985: Medium-Range Weather Forecasts - the first 10 years, Rep. from European Centre for Medium-Range Weather Forecasts, 67-86.

May, R.M., 1976: Theoretical Ecology, Blackwell Scientific Publ., 317 pp.

May, R.M. and W.J. Leonard, 1975: Nonlinear aspects of competition between three species, SIAM, Jour. of Appl. Math., 29, 243-252.

Phillips, N.A., 1956: The general circulation of the atmosphere: A numerical experiment, Quart. Jour. Roy. Met. Soc., 82, 123 164.

Platzman, G.W., 1960: The spectral form of the vorticity equation, Jour. of Meteor., 17, 635-644.

Plaut, G. and R. Vautard, 1994: Spells of low-frequency oscillations and weather regimes in the Northern Hemisphere, Jour. Atm.Sci., 51 210-236.

Poincaré, H., 1893: Les Méthodes nouvelle de la mechanique celeste, Paris, Gauthier-Villar.

Poincaré, H., 1912: Science et Méthodes, Paris, Flammarion.

Thompson, P.D., 1957: Uncertainty of initial state as a factor in predictability of large-scale atmospheric flow pattern, Tellus, 9, 275-295.

Wiin-Nielsen, A., 1961: On short- and long-term variations in quasi-barotropic flow, Mo.Wea. Rev, 89, 461-476.

Wiin-Nielsen, A., 1991: Comparison of low-order atmospheric systems, Atmósfera, 5, 135-155.

Wiin-Nielsen, A., 1992: Low-order baroclinic models forced by meridional and zonal heating, Geophysica, 27, 13-40.

Wiin-Nielsen, A., 1996: A note on longer term oscillations in the atmosphere Atmósfera, 9, 222-240.

Wiin-Nielsen, A., 1997: 'Everybody talks about it...', Math.-Phys. Medd., 44:1, Danish Royal Society for Science and Humanities, 96 pp.

Wiin-Nielsen A., 1997: On intermonthly oscillations in the atmosphere, Atmósfera, 10, 23-42.

Wiin-Nielsen, A., 1998: On the stable part of the Lorenz attractor, Atmósfera, 11, 61-73.

Wiin-Nielsen, A., 1998: Limited predictability (in danish), Kvant, 9, 21-25.

Wiin-Nielsen, A, 1999: Steady states and transient solutions of the nonlinear forced shallow water equations in one space dimension, acc. for publ., Atmósfera, 12.